sustainability

IMPACT FACTOR 3.3

CITESCORE 6.8

Article

Behavior of the Electricity and Gas Grids When Injecting Synthetic Natural Gas Produced with Electricity Surplus of Rooftop PVs

Andrea Ademollo, Carlo Carcasci and Albana Ilo

Special Issue
Sustainable Energy Transition: The Role of Renewable Energy and Power Systems—Current Trends and Challenges

Edited by
Prof. Dr. Christopher Koroneos and Dr. Evanthia A. Nanaki

MDPI

https://doi.org/10.3390/su16229747

sustainability

Article

Behavior of the Electricity and Gas Grids When Injecting Synthetic Natural Gas Produced with Electricity Surplus of Rooftop PVs

Andrea Ademollo [1,*], Carlo Carcasci [1] and Albana Ilo [2]

[1] Department of Industrial Engineering, Università degli Studi di Firenze, 50139 Firenze, Italy; carlo.carcasci@unifi.it
[2] Institute of Energy Systems and Electrical Drives, TU Wien, 1040 Vienna, Austria; ilo@ea.tuwien.ac.at
* Correspondence: andrea.ademollo@unifi.it

Abstract: Distributed generation and sector coupling are key factors for economic decarbonization. Because gas networks have a large storage capacity, they have attracted the attention of power engineers to use them to increase the flexibility and security of supply in the presence of renewable and distributed energy resources. This paper makes the first attempt to integrate the electricity and gas systems to fill available gas storage facilities with synthetic natural gas on a large scale. This synthetic natural gas can then be used to operate gas turbines and to compensate for the fluctuating production of renewable energy sources. The *LINK*-holistic architecture, which integrates renewable and distributed energy resources, is used in this work. It facilitates sector coupling, which means power-to-gas and gas-to-power, throughout the entire power grid and at the customer level. This work is limited to investigating the power-to-gas process at the prosumer level. The electricity surplus of rooftop PVs is used to produce synthetic natural gas, fed into the gas grid after covering the local gas load. The behaviors of the electricity and gas grids are investigated. Results show that electricity prosumers may also become prosumers of synthetic natural gas. The current unidirectional gas grids should be upgraded with compressors at pressure reduction groups to turn them bidirectional, allowing synthetic natural gas storage in the existing large gas storage appliances after considering the pipes' linepack effect. The proposed solution could make it possible to fill the underground storage plants in summer, when the electricity and synthetic natural gas production exceed electrical and gas demand, respectively.

Keywords: flexibility of supply; security of supply; sector coupling; gas grid; electricity grid; rooftop photovoltaic; power-to-gas; synthetic natural gas (SNG); *LINK*-Solution

check for updates

Citation: Ademollo, A.; Carcasci, C.; Ilo, A. Behavior of the Electricity and Gas Grids When Injecting Synthetic Natural Gas Produced with Electricity Surplus of Rooftop PVs. *Sustainability* **2024**, *16*, 9747. https://doi.org/10.3390/su16229747

Academic Editors: Christopher Koroneos and Evanthia A. Nanaki

Received: 6 September 2024
Revised: 11 October 2024
Accepted: 1 November 2024
Published: 8 November 2024

1. Introduction

Environmental protection policies and overall climate commitments require the decarbonization of all sectors of the economy. Energy systems are undergoing a transformation process in which their integration will play a significant role. Integrating energy sectors on a regional scale is expected to impact energy systems' reliability significantly, operating costs, and environmental performance [1]. This transformation presents various challenges, necessitating a holistic approach [2].

This paper focuses on end-use sector coupling to integrate the electricity and gas systems. It investigates the possibility of introducing the distributed production of green synthetic natural gas (SNG), whose adequate technologies are evolving, and feeding it into the low-pressure pipelines.

1.1. Literature Review in Electricity Grids

In recent years, the power sector has experienced a dramatic increase in distributed generation (DG) due to the energy crisis. The most widespread technology is rooftop photovoltaic (PV) systems. However, distribution system operators (DSOs) cannot meet the public's need for PV systems due to severe voltage and thermal limit violations caused by the reverse flow of currents [3]. Exceeding the voltage upper limit in the DG presence in radial structures of distribution networks has been known for a long time [4–8]. It quickly became apparent that reactive power support could increase the hosting capacity of radial networks on DGs [9–11]. However, the problem of exceeding thermal limits remains and requires infrastructure expansion; transformers, lines, cables, etc., must be adapted, or sector coupling solutions may be considered [12].

Existing gas infrastructure offers many opportunities for coupling with the power system infrastructure. It serves a large portion of the EU territory, allowing energy transfer over long distances at a low cost and with reduced energy losses. The gas grid can provide large seasonal energy storage capacities.

1.2. Literature Review on Gas Grids

Gas grids are moving towards partial decarbonization by injecting substitute natural gases (NGs). The development and deployment of substitute NG are partially linked to the rapid growth of electric renewable energy sources. A viable solution to integrate their excess is converting electricity into H_2. Direct H_2 injection into existing NG pipelines has been proposed and extensively examined in the literature as a viable approach [13,14]. Deymi-Dashtebayaz et al. [15] analyzed the effect of $1 \div 10$ vol% H_2 injection into the gas grid on all important NG properties. Guzzo et al. [16] determined the maximum permissible percentage of hydrogen blending as a function of gas composition, emphasizing the difficulty to define a universal hydrogen limit.

Among the numerous envisioned applications for hydrogen in the decarbonization of the energy system from the customer plant (CP) perspective, seasonal energy storage is usually considered one of the most likely options (a CP is a place where electricity or gas is produced or consumed, or both produced and consumed). Lubello et al. [17] investigated residential storage systems and their possible applications for different geographical conditions in Italy, demonstrating how such systems are not generally economically competitive for a single dwelling, although they can sometimes ensure energy independence. Instead, H_2 can be a viable solution to decarbonize the hard-to-abate sectors, as assessed by Mati et al. [18] and by Ademollo et al. [19] who provided a techno-economic analysis for the conversion of a conventional cogeneration system for a paper mill application. Mati et al. focused on a 100% hydrogen-fueled gas turbine system, while Ademollo et al. examined a 100% hydrogen-fueled solid oxide fuel cell system demonstrating the economic feasibility of these solutions for such applications.

H_2 can also be combined with CO_2 to produce SNG. The most common application to produce it concerns the thermochemical process employing different catalytic reactors [20]. Methanation is a chemical transformation, often referred to as the Sabatier reaction, offering a promising solution for mitigating greenhouse gas emissions, as it not only converts CO_2 into a valuable fuel source but also integrates with the concept of power-to-gas (P2G) technology, enabling the storage of excess electricity within the natural gas grid [21]. Becker et al. [22] discussed a power-to-SNG plant's design and techno-economic analysis for producing SNG from CO_2 and renewable hydrogen. Tang et al. [23] explored the efficient utilization of CO_2 in P2G systems, including converting CO_2 into various end products such as SNG.

1.3. Literature Review on Coupling the Electricity and Gas Grid

Sector coupling between electricity and gas grids, particularly with respect to gas injection into the gas grid, has been a topic of increasing attention in the literature. Quarton et al. [24] reviewed real-life projects related to P2G for injection into the gas grid providing insights on the integration of gas injections at various points of the network. Gui-Xiong et al. [25] focused on the coupling between an electricity power system and an NG system combined with distributed gas injections with a regional integrated energy system as the background.

Held et al. [26] discussed the synthesis of SNG and its injection into the natural gas grid, focusing on catalytic methanation in catalytically coated metallic honeycomb reactors and slurry bubble column reactors. Giglio et al. [27] explored the integration of high-temperature electrolysis and methanation for SNG production. Estermann et al. [28] investigated the feasibility of implementing P2G systems to absorb surplus solar power from electricity distribution networks and carbon dioxide from biomass anaerobic digestion plants to produce synthetic methane at the low-voltage level.

The holistic *LINK* architecture organizes cross-sector sector coupling across all voltage levels within power grids and end-user sector coupling [29], thereby enabling a joint analysis of electricity and gas grids [30].

This study focuses on the CP level and the end components of the networks, specifically the low-voltage (LV) feeders and low-pressure (LP) pipelines, respectively, for electricity and gas. For the first time, it jointly investigates both power and gas grids as well as power and gas appliances at the CP level providing a structured architecture that enables its reproducibility across all voltage and pressure levels. This paper is organized as follows: Section 2 gives an overview of the energy systems, compares the electricity and gas systems, and introduces the holistic *LINK* architecture for electricity and gas grid coupling. The setup description follows the premises for its realisation, corresponding to the modeling and scenario definition. Section 3 discusses the behavior of electricity and gas grids when coupled. Finally, Section 4 discusses in detail the results of this work, technological development, and future research perspectives.

2. Materials and Methods

Figure 1 shows the investigation methodology used to perform this work. The paper investigates electricity and gas grids to compare them, identifying similarities and differences. A holistic analysis identifies the coupling possibilities between the electricity and gas grids, followed by adequate simulation modeling. Finally, simulation results are investigated.

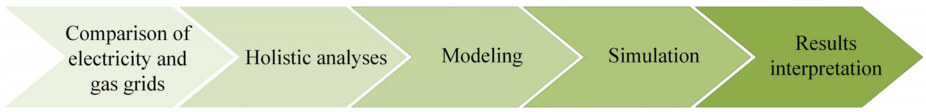

Figure 1. The investigation methodology.

2.1. Structure of Energy Systems

Energy systems supply energy to end-users. They constitute the energy vectors, such as electricity, gas, heat, etc., in the secondary economy sector [31]. They are widely distributed within a continent and sometimes between continents with above- and below-ground pipes, overhead lines and cables, terrestrial or marine. Energy Systems Integration (ESI) coordinates the operation and planning of energy systems to deliver reliable, cost-effective energy services with minimal environmental impact [32]. It connects energy systems of various vectors within the second sector, i.e., Cross different vectors of the energy utilities such as electricity, heating and cooling, and gas. The cross-vector sector coupling integrates these various energy infrastructures and vectors. In contrast, the end-use sector coupling [33] involves different infrastructures, such as electricity, gas, etc., at the customer plant level.

Figure 2 shows the integrated energy systems through sector coupling, as the *LINK*-Solution postulates. The coupling through the electricity, gas, and thermal networks is realized through the coupling components. For example, electrolyzers combined with methanation reactors couple the electricity grid with the gas network, enabling the P2G process. Fuel cells couple the electricity with the gas grid, allowing the gas-to-power (G2P) process. Heat pumps couple the electricity and heat networks, enabling the power-to-heat (P2H) process. The coupling between the gas and heating networks is realized through the gas condensing boilers and CHPs that allow the gas-to-heat (G2H) process. Through power-to-X solutions, sector coupling contributes directly to the abatement of emissions in multiple sectors of the economy by providing big storage capability, an element which is central in the *LINK* architecture. It is categorized into three categories: "Cat. A", E-St.-A, the stored energy is injected at the charging point of the grid, such as pumped hydroelectric storage, stationary batteries, etc. In "Cat. B", E-St.-B, the stored energy is not injected back at the charging point on the grid, such as power-to-gas (P2G), batteries of e-cars, etc. In "Cat. C", E-St.-C, the stored energy shortly reduces the electricity consumption at the charging point, such as cooling and heating systems (consuming devices with energy storage potential). In this work, it is treated as the Cat. B of storage.

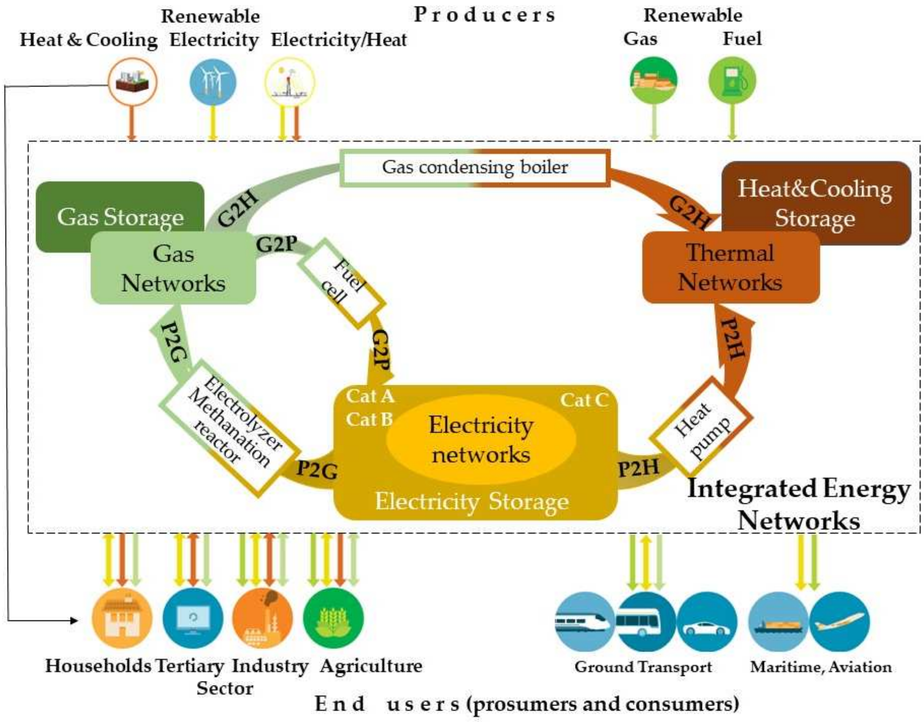

Figure 2. Integrated energy systems through sector coupling, as given by the *LINK*-Solution [34].

2.2. Comparison Between Electricity and Gas Grids

Electricity and gas have some different essential characteristics. Electricity propagates in wires at almost the speed of light, while natural gas travels up to 100 km/h [35]. Gas system operators control pipelines, and unlike electricity systems, supply and demand do not need to be fully balanced in real-time and while electricity can be transformed into other forms of energy for storage, such as chemical potential in batteries or potential energy in pumped hydroelectric storage, it is not inherently storable as a commodity. Instead, gas may be stored in tanks and pipelines. The gas systems in Europe have a long-term storage capacity in the TWh range, which makes it very attractive for the renewable electrification of all energy vectors [36]. Examples are compressed natural gas (CNG), liquefied natural gas (LNG), and underground gas storage (UGS). Active and reactive power circulates in the electricity systems, where the reactive power is a byproduct of AC systems. Differently, gas systems circulate only NG, which the end-customers consume. Natural gas flow in one pipeline can be controlled independently of the other gas network components. While electricity flow can evolve in both directions due to transformer characteristics, the gas flow is typically unidirectional. Controlling the power flow, e.g., in one transmission line segmentally, is technically not feasible because of the interdependencies within the power system. In the electricity grid, current flow can only be interrupted (using circuit breakers or fuses), whereas in the gas grid, the flow rate can be adjusted via lamination valves, which increase localized pressure losses, thereby reducing pressure and consequently diminishing the flow rate. Despite all this, there are many similarities in the structure of gas and electricity systems. The similarity between electric and gas network structures has been known for a long time; even the natural gas load flow problems are solved using the electric load flow techniques [37].

The traditional power and gas systems have the same rough structure. Both systems deliver electricity or natural gas from the big power plants or gas wellheads to end-electricity and end-gas customers through transmission and distribution grids or pipes, as Figure 3 shows.

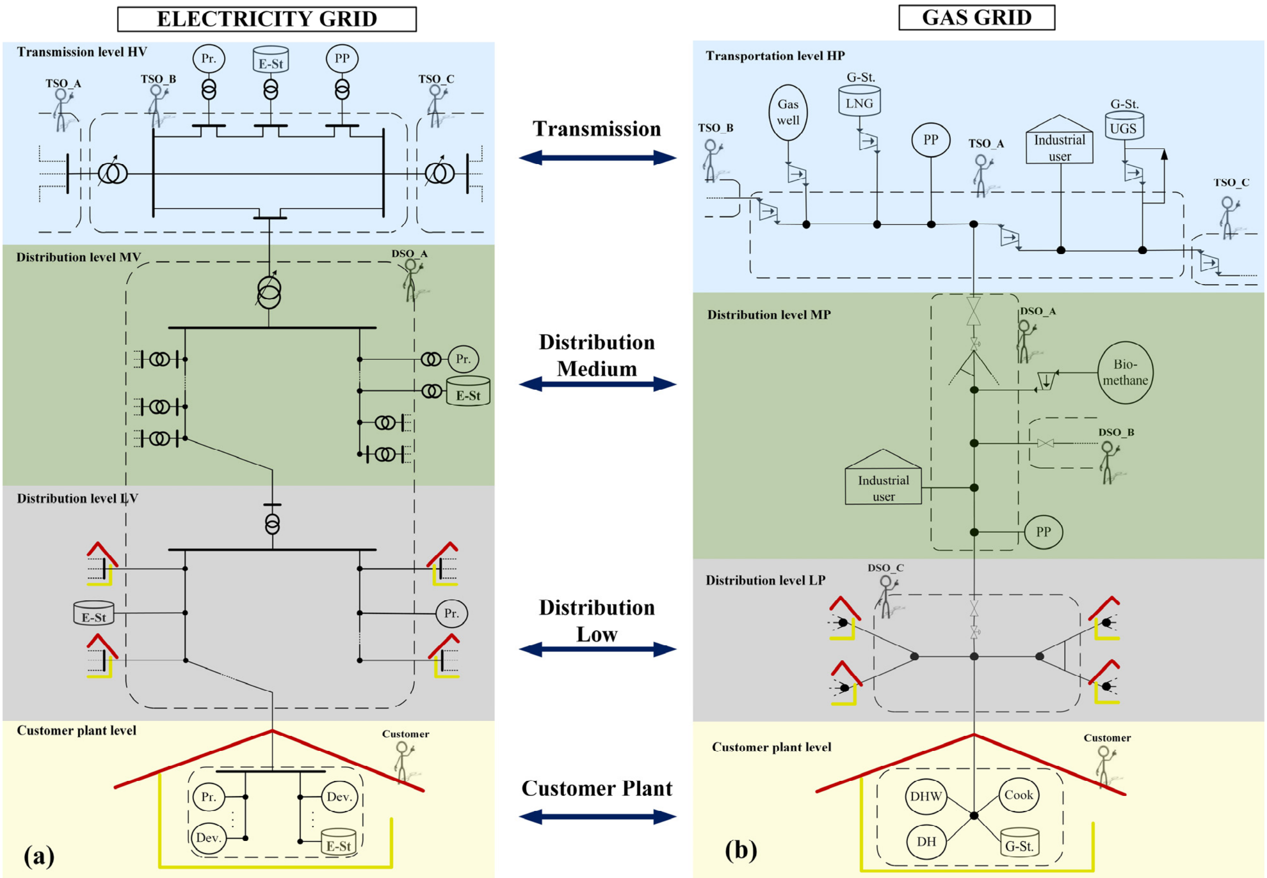

Figure 3. Electricity and gas grid structures. (**a**) Electricity grid structure. (**b**) Gas grid structure.

The gas wells and big power plants are located at sites distant from the load centers. Figure 3a shows the structure of electricity grids categorized into transmission (very high and high voltage) and distribution (medium and low voltage) grids. The same categorization is relevant for the gas grid as shown in Figure 3b, wherein transmission includes the high, while in distribution, the medium- and low-pressure pipes. The grid symbols used in Figure 3 are summarized in Appendix A, Table A1. An analogy exists between the electrical busbars, mechanical, and electrical connections of at least two conductors and the nodes realised by welding different pipelines: they connect two parts used to transmit and distribute electricity or gas, respectively. Power lines and pipelines can be laid aboveground or underground. The analogous quantity of the voltage is the pressure, and that of the active power flow is the gas flow. In analogy to the transformer stands the compressor. The transformer analogy, which changes the voltage level in both directions, shows the compressor increasing the pressure and the valve decreasing it.

2.3. LINK Architecture for Electricity and Gas Grid Coupling

Currently, each energy system, be it electricity, gas, or heat and cooling, works separately, each with its design guidelines. The holistic approach helps adapt their designs to have an overall synthesis and enable substantial harmonized operation between the vectors and environmentally friendly growth. Also, within each energy vector that may extend over a continent, traditionally, it is not used in any holistic approach.

The newly developed holistic *LINK* architecture for electricity looks at power systems and customer plants as one interconnected electromagnetic entity, understanding the bigger picture by thinking outside the transmission or distribution box. This approach gives equal importance and an overall shared purpose to every part of the power system and customer plants and, therefore, can ensure the power industry is running to its full potential. No holistic approach is used for gas systems to harmonize their operation and planning processes.

Figure 4 shows an extension of the *LINK* architecture with the knowledge gained in Section 2.2. It helps to identify the coupling possibilities between the electricity and gas systems. Both systems can be coupled grid-wide through coupling components (CC) to realize the cross-vector sector coupling and at the CP level to realize so-called end-user sector coupling. The cross-vector sector coupling may be realized in different levels as follows: The extra high-voltage (EHV) or high-voltage (HV) grids may be coupled with HP gas grids; the medium-voltage (MV) grids may be coupled with MP gas grids; and the low-voltage (LV) grids may be coupled with LP gas grids. The SNG produced using the electricity surplus in the power system may be stored in the "G-St." available in the gas vector and can be used to operate gas turbines to compensate for the fluctuating production of renewable energy sources.

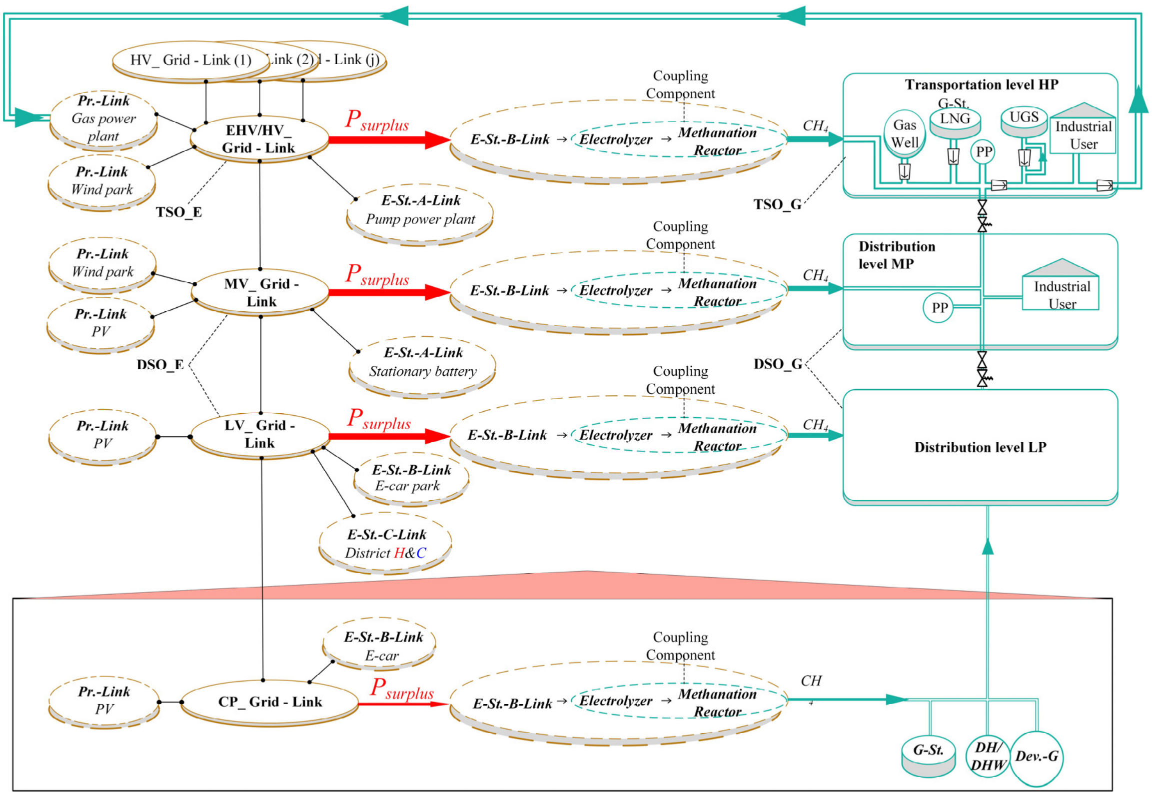

Figure 4. P2G and G2P processes embedded in the *LINK* architecture.

From the design point of view, it is possible to couple the grids at the end-user level in the customer plants connected with the gas grid. The electricity surplus of rooftop PVs may also be used to produce SNG, which can be injected into the gas grid and, in the given case, stored in the G-St. available in the gas vector. However, many questions arise regarding the coupling's technical feasibility and economic viability at the CP level, which are discussed in more detail in this paper.

2.4. Premises for the Realization of End-Use Sector Coupling

The central premise to realize the end-use sector coupling [33] is the presence of surplus electricity generated from renewable sources in the CP site. The electricity grid has limitations in uptaking the electricity surplus produced by the distributed generation or prosumers.

2.4.1. Limitations of the Grid to Uptake the Electricity Surplus of Distributed Resources

Figure 5 shows the critical parameters for the uptake capacity of rooftop PV facilities in an LV subsystem and the countermeasures for their maximum expansion [12].

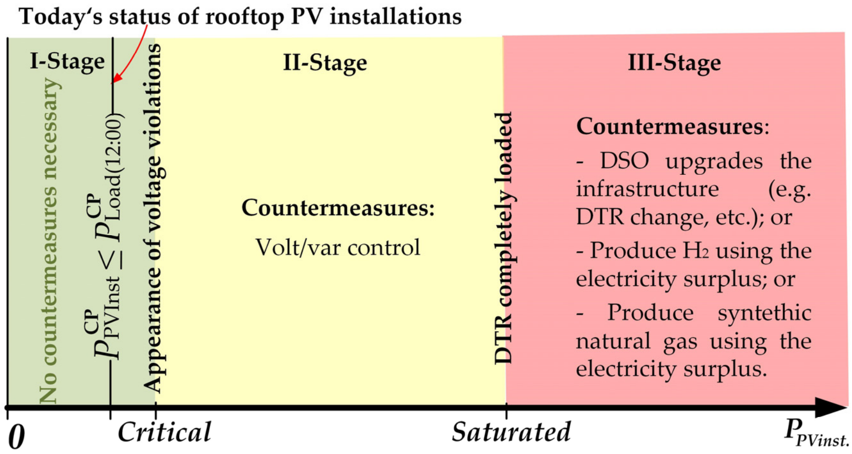

Figure 5. Critical parameters for the uptake capacity of rooftop PV facilities in an LV subsystem and the countermeasures for their maximum expansion [12].

Three cases are figured out depending on the extent of the electricity surplus. In the first case, the green area, electrical surplus does not provoke the violation of the upper voltage limit up to a "Critical" value of the PV installations. In the second case, the yellow area, voltage violations appear, and countermeasures such as Volt/var control are needed to guarantee the reliable and sustainable operation of the power grid up to the "Saturated" value on PV installations. In the third case, the red area, where the grid is saturated in up-taking distributed generation, the infrastructure is overloaded, meaning that the thermal limits for transformers, overhead lines, and cables are reached. Additional countermeasures are required to ensure the secure utilization of the infrastructure. The countermeasures can be diverse and realized by different stakeholders. The DSO may reinforce the infrastructure (e.g., change the distribution transformer (DTR), etc.), or the electricity surplus may be stored in a battery for power-to-power (P2P) storage. At the LV level, short-term storage via battery banks charging during the daytime and discharging at night is a conventional approach [37]. However, when the renewable penetration reaches high levels, the effectiveness of such P2P storage diminishes [38,39]. This is because on many days of the year, the amount of excess solar generated during the daytime exceeds the following night's electricity demand, so the requirement to discharge the stored energy to the power system forces the use of an extreme storage capacity if solar curtailment is to be avoided altogether. Therefore, P2P storage technologies are considered stable for energy storage at low PV penetration levels [28]. Thus, P2G will be required to access the very large capacity of the gas grid if high PV penetrations are to be achieved.

2.4.2. Power-to-Gas Potential at Customer Plant Level

A possible solution is using rooftop surplus PV to generate H_2 at the CP level through an electrolyzer. However, integrating H_2 into household appliances and the existing gas grid poses significant challenges. The current infrastructure, for the most part, is not equipped to accommodate H_2 due to the risk of embrittlement [40]. Furthermore, even if the infrastructure were H_2-compatible, the H_2 volume content of the NG-H_2 mixture cannot exceed 15 ÷ 20% [41]. Therefore, this study proposes a solution to these challenges: upgrading the produced H_2 to SNG. This process involves the conversion of CO_2, sourced from a pressurized tank, into SNG with the aid of H_2 in a small-scale methanation reactor. The resulting SNG is then utilized to meet the local gas load before being injected into the LP gas grid.

P2G systems are showcased in various countries, demonstrating the injection of H_2 or SNG into gas grids [42,43]. Stakeholders and policymakers still need to agree on the remuneration framework for SNG injection from the CP level and targets for capturing rather than wasting excess solar. Several factors should be considered when implementing P2G plants at the CP to determine the feasibility of achieving any target for excess solar energy capture. These factors include:

- The design and layout of the region's electricity distribution network, including the number, capacities, and locations of MV/LV transformers, as well as the length of LV feeders connecting various CPs;
- The market structure to consider small distributed electricity and gas resources and the maturity of the CO_2 market;
- The feasibility of installing P2G plants close to CPs;
- The layout and design of local gas distribution zones and the transient variation in natural gas flow rates that occur throughout the day/year at potential sites for SNG injection;
- The all-around feasibility of the solution, considering the energy trilemma.

2.4.3. General Procedure for Realizing the P2G Process

Figure 6 shows the general approach of the P2G process at the CP level. The procedure starts with determining the PV production, P_{PV}, profile in the study area, followed by identifying the load profile, P_{Load}, of the customer type (commercial, residential, etc.) for which the P2G process will be established and implemented. Depending on the specific conditions and countermeasures taken in the power grid, it may take off part of the excess power, $P_{Sp.}^{Grid}$. The power surplus, $P_{Sp.}$, is calculated for each time point t as given in Equation (1).

$$P_{Sp.}(t) = P_{PV}(t) - P_{Load}(t) - P_{Sp.}^{Grid}(t) \tag{1}$$

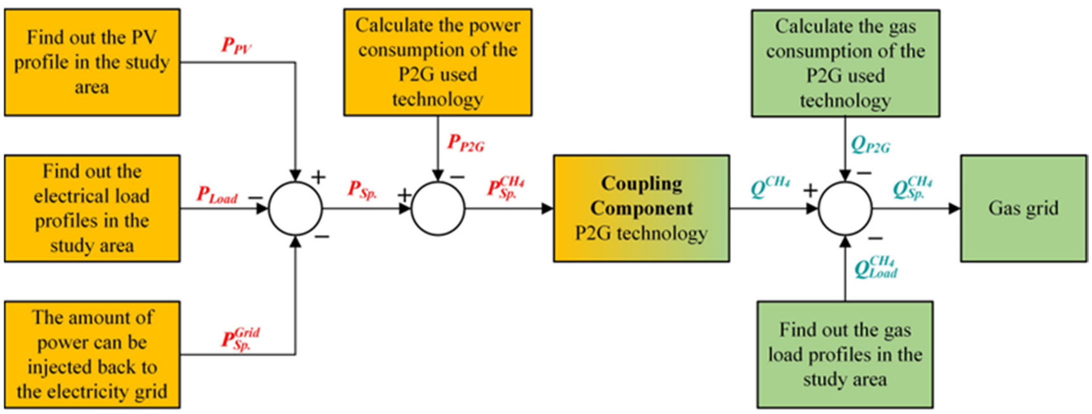

Figure 6. General procedure for realizing the P2G process at the CP level.

Calculate the power needed to operate the P2G technology used as CC, P_{P2G}, to define the net surplus of electricity that can be used to produce SNG, $P_{Sp.}^{CH_4}$ in Equation (2).

$$P_{Sp.}^{CH_4}(t) = P_{Sp.}(t) - P_{P2G}(t) \tag{2}$$

The CC will produce SNG, Q^{CH_4}, which can be used to supply the CP gas load. In this paper, SNG will also be referred to simply as CH_4, as both nomenclatures denote the same compound. The profile of the gas load will be determined, and the amount of gas that may be injected into the LP pipe is calculated as in Equation (3).

$$Q^{CH_4}_{Sp.}(t) = Q^{CH_4}(t) - Q^{CH_4}_{Load}(t) - Q^{CH_4}_{P2G}(t) \tag{3}$$

For the entire simulation process, a program has been written in Python where the modeling of the electrolyzer and methanation reactor (Section 2.6.2) has been carried out to find PV surplus and SNG production. These output values have been used as input in PSS Sincal [44], a comprehensive, high-quality software solution for network planning requirements. PSS Sincal provides detailed modeling capabilities for electrical networks across high-, medium-, and low-voltage levels, and additionally supports pipe network calculations for water, gas, and district heating and cooling applications. So, this study utilized PSS Sincal to conduct steady-state simulations to understand how distributed injections of electricity and SNG impact the electricity grid voltage profiles and the gas grid pressure/velocity profiles, respectively. Additionally, the analysis of the linepack effect, which is the possibility of exploiting the LP pipeline's storage capability resulting from SNG's injections into the LP grid, has been entirely modeled in Python and described in detail in Appendix C.

2.5. Setup Description

The study examines a theoretical residential area connected to both electricity and gas infrastructure, as Figure 7 shows. The electricity grid includes a 250 kVA distribution transformer (DTR) which connects a 0.4 kV LV grid to a 10 kV MV feeder. While, for the gas grid, a pressure reduction group (PRG) connects a 30 mbar LP grid with a 5 bar MP pipeline. The LV feeder and the LP pipeline have the same length of 600 m. Twenty identical residential CPs are connected to both grids at ten equidistant connection points of 60 m. CPs are connected to the LV and LP grids through a 10 m cable and 10 m pipe.

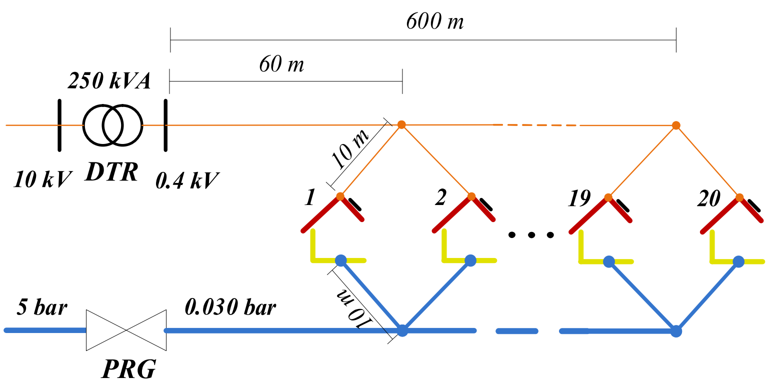

Figure 7. Scheme of the analyzed case study.

Figure 8 depicts a schematic representation of the electrical and gas devices considered in each CP. Regarding electricity, each CP has a PV facility and electrical devices. Regarding gas, each CP has gas devices needed for cooking and domestic hot water (DHW). The coupling component is P2G technology. No storage appliances have been considered in this study. The power flow is shown in red, while the gas flow in turquoise.

P2G technology at the CP level is postulated as a composition of two coupling components: the electrolyzer and the methanation reactor, as highlighted in Figure 9.

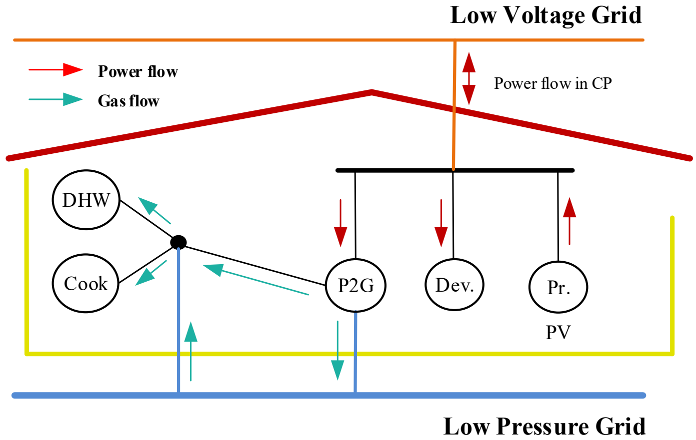

Figure 8. Schematic representation of the electrical and gas devices considered in each CP.

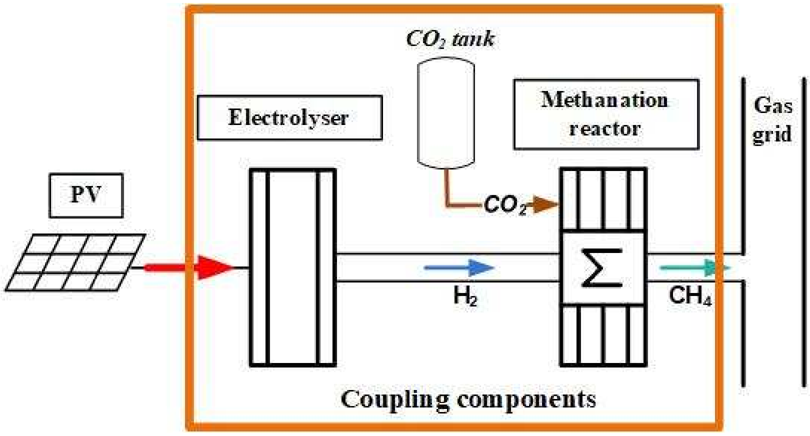

Figure 9. P2G technologies inside each CP.

2.6. Modeling

In this section, the modeling of the main components is carried out.

2.6.1. Electricity and Gas Grids

Figure 10 emphasizes the electric and thermal profiles. PV production profile is typical of summer PV production in northern Italy, thus being characterized by a bell shape with almost 14 h of light. The electric load profile represents a typical four-person household, peaking at 20:00 h. The gas load profile, also typical for a four-person household, reflects the need for DHW and gas cookers during summer months when DH is not required.

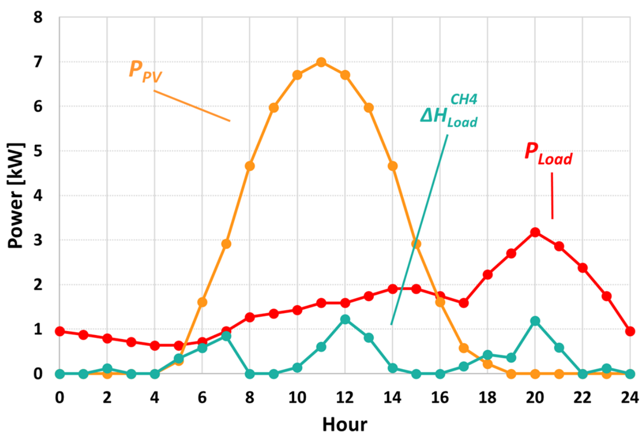

Figure 10. PV production, electric load, and thermal load profiles for each CP, July, Turin.

Because of the absence of storage appliances, both loads can be covered only when production and consumption are simultaneous.

Maximum power values for the case under consideration are represented in Table 1:

Table 1. Maximum power values.

Parameter	Description	Value
P_{Load}^{Peak}	Peak electric power	3 kW
P_{PV}^{Peak}	Peak PV power	7 kW
$\Delta H_{Load}^{CH4,Peak}$	Peak thermal power	1.2 kW

The models used for the elements of electricity and gas grids are PSS Sincal ones and are described in Appendices B and C, respectively. The simulated electricity and gas grid parameters are chosen following the state-of-the-art of a general LV and LP grid, respectively. Concerning the gas grid, the nominal pressure varies with the analyzed scenario and the selected pipeline diameter (Section 2.7.1). At the same time, load consumption and flow supply values depend, respectively, on the maximum gas consumed and maximum SNG injectable after coupling, and they change with the selected scenario. The modeling of the linepack effect is described in Appendix C. Figure 11 shows electricity grid voltage limits and gas grid pressure limits at the CP level as well as the coupling components under study.

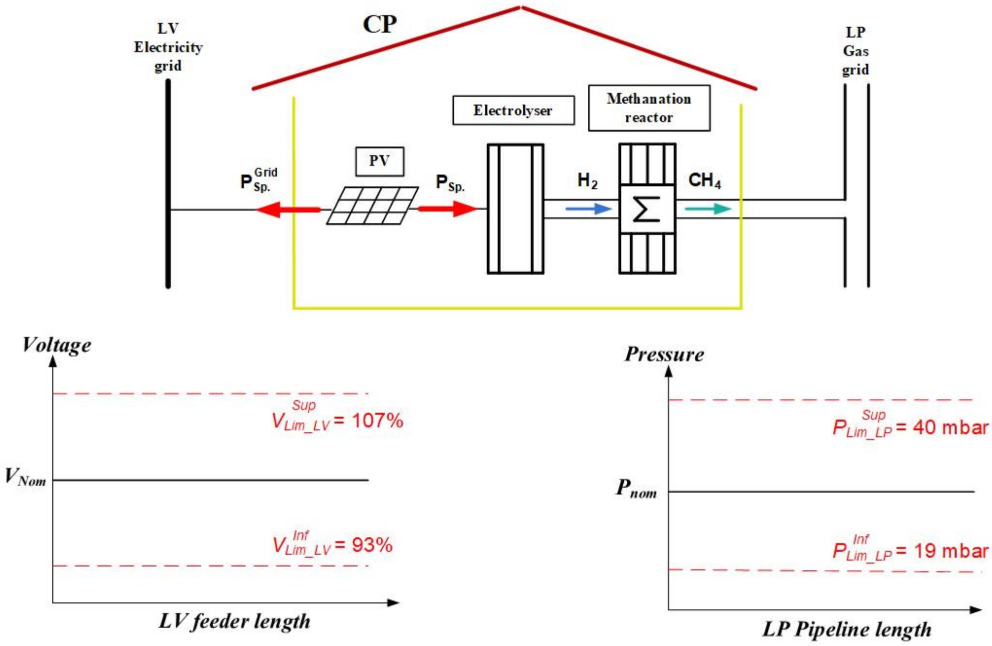

Figure 11. End-use sector coupling with voltage and pressure limits in electricity and gas grids.

2.6.2. Coupling Components

Electrolyzer modeling

Electrolysis of H_2O dissociates H_2 and O_2 absorbing electricity through an electrolyzer, as represented in Equation (4).

$$H_2O_{(l)} = H_{2(g)} + \frac{1}{2}O_{2(g)} \tag{4}$$

The plant structure of the electrolyzer is highlighted in Figure 12.

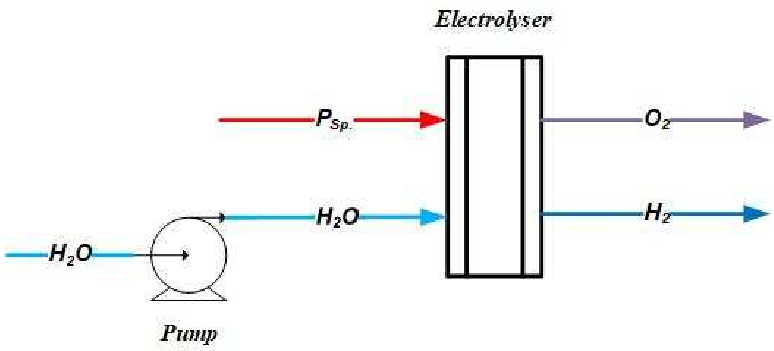

Figure 12. Electrolyzer operation scheme.

The electrolyzer needs to be supplied with pressurized H_2O, necessitating the inclusion of a pump in the plant. Once the type of electrolyzer and the electricity surplus ($P_{Sp.}^{CH_4}$) are known, the H_2 volumetric flow rate production (Q_{H_2}) can be calculated as in Equation (5).

$$Q_{H_2} = \frac{P_{Sp.}^{CH_4}}{F_{H_2}} \tag{5}$$

where F_{H_2} is the hydrogen conversion rate (kWh/Nm^3).

But, to produce H_2, the electrolyzer must be supplied with pressurized H_2O, so additional work from the pump must be considered leading to the iterative calculation represented below to calculate the real H_2 flow rate producible as assessed by Equations (6)–(9):

$$mol_{H_2} = \frac{Q_{H_2} \times \rho_{H_2}}{Mw_{H_2}} \tag{6}$$

$$mol_{H_2O} = mol_{H_2} \tag{7}$$

$$P_{Pump}^{P2G} = \frac{mol_{H_2O} \times Mw_{H_2O} \times \left(P_{el}^{Pr} - P_{n}^{Pr}\right)}{\rho_{H_2O}} \tag{8}$$

$$Q_{H_2\_new} = \frac{P_{Sp.}^{CH_4} - \frac{P_{Pump}^{P2G}}{\eta_{pump} \times \eta_{Gen}}}{F_{H_2}} \tag{9}$$

where mol, Mw, P_{el}^{Pr}, P_{n}^{Pr}, η_{pump}, η_{Gen}, and P_{Pump}^{P2G} are, respectively, the number of moles of a chemical substance (mol), the molecular weight of a chemical substance (g/mol), the absolute pressure of the electrolyzer (Pa), the normal pressure (Pa), the pump efficiency (-), the generator efficiency (-), and the power requested by the pump to compress H_2 (kW).

Once the new hydrogen flow rate production ($Q_{H_2\_new}$) is found, the iterations restart from Equation (6) until the difference between Q_{H_2} and $Q_{H_2\_new}$ is lower than 10^{-7}.

Methanation reactor modeling

Methanation is a chemical transformation, often referred to as the Sabatier reaction, offering a promising solution for mitigating greenhouse gas emissions, as it not only converts CO_2 into a valuable fuel source but also integrates with the concept of P2G technology, enabling the storage of excess electricity within the natural gas grid [20]. Smaller decentralized methanation facilities are required because of the demand for high flexibility, limited feed-in capacities, and public acceptance. An essential criterion for the profitability of small-scale SNG facilities is a low process complexity, which must be considered for the whole process chain [45]. To run this process, a compressed CO_2 tank is necessary. Compressed CO_2 is already widely used in various industries, including food and beverage, agriculture, and manufacturing. Gas supply companies typically sell it, and it can be purchased in multiple quantities, from small cylinders to large tanks [46,47]. The methanation reaction of CO_2 is an exothermic catalytic reaction. Operation typically occurs at temperatures ranging from 150 °C to 550 °C and pressure between 1 and 30 bar depending on the catalyst, as specified in Equation (10).

$$CO_2 + 4H_2 = CH_4 + 2H_2O \tag{10}$$

The plant structure of the methanation reactor is highlighted in Figure 13.

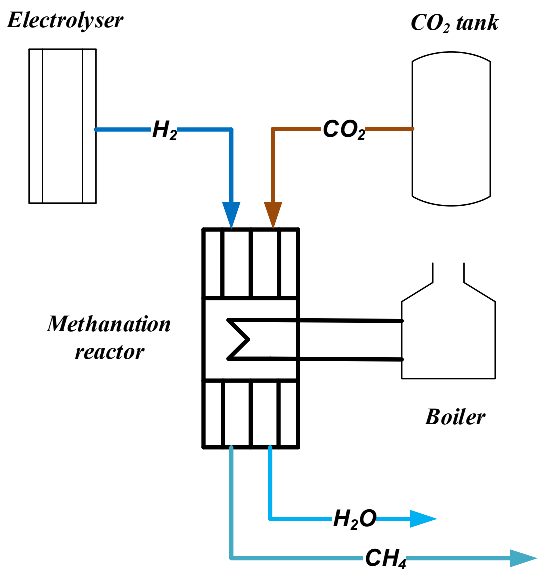

Figure 13. Methanation reactor operation scheme.

As the methanation reactor's operative pressure equals the electrolyzer's one, no compressor is needed to compress hydrogen up to that pressure. Additionally, it has been supposed that CO_2 pressure inside the tank is equal to methanation's one. Thus, no additional electric power is necessary between the electrolyzer and the methanation reactor. Therefore, the only additional energy needed is thermal energy, which increases due to the typically higher operating temperature of the methanation process compared to that of the electrolyzer (Equations (11) and (12)).

$$\Delta H_{H_2} = \frac{(\dot{m}_{H_2} \times c_p \times (T_{met} - T_{el}))}{\eta_{boiler}} \tag{11}$$

$$\Delta H_{CO_2} = \frac{(\dot{m}_{CO_2} \times c_p \times (T_{met} - T_{tank}))}{\eta_{boiler}} \tag{12}$$

where ΔH, $\dot{m}$, c_p T_{el}, T_{met}, T_{tank}, and η_{boiler} are, respectively, the thermal power (kW), the mass flow rate (kg/s), the specific heat at constant pressure (J/kgK), the temperature (K) of the electrolyzer, the methanation reactor and the tank, and the boiler efficiency (-).

Since the H_2 mass flow rate is preserved, it is possible to find the SNG normal volumetric flow rate $Q^n_{CH_4}$ (Nm^3/h) produced by Equation (14).

$$Q_{CH_4} = \frac{\frac{mol_{H_2}}{4} \times Mw_{CH_4} \times F_{CO_2}}{\rho_{CH_4}} \tag{13}$$

$$Q^n_{CH_4} = Q_{CH_4} \times \left(\frac{P^{Pr}_{met}}{P^{Pr}_{n}} \times \frac{T_n}{T_{met}} \right) \tag{14}$$

where P^{Pr}_{met} and F_{CO_2} are, respectively, the methanation reactor's absolute pressure (Pa) and the CO_2 conversion efficiency factor (-). The last parameter is dependent on the reactor's operating conditions (temperature and pressure) [48].

To simulate the CCs, it has been assumed that the NG temperature in the pipe, H_2O temperature taken from the aqueduct, and CO_2 temperature in the tank is equal to the ambient one, i.e., 15 °C.

Then, the following assumptions have been made (Table 2):

Table 2. Auxiliary components' characteristics.

Parameter	Description	Value
η_{pump}	Pump efficiency	80%
η_{Gen}	Generator efficiency	95%
η_{boiler}	Boiler efficiency	85%

An Anion Exchange Membrane (AEM) electrolyzer has been selected. It is realized by the 'Enapter' company specifically for house scales and it has the following characteristics (Table 3):

Table 3. AEM electrolyzer characteristics [49].

Parameter	Value
P_{el}^{Pr}	8 bar
T_{el}	50 °C
F_{H_2}	4.8 kWh/Nm^3
Peak power consumption	3 kW
V	200 ÷ 230 V (AC)
f_n	50 ÷ 60 Hz
Ambient operative temperature range	5 ÷ 45 °C

Since it has a peak power consumption of 3 kW, two modules are needed because the PV electricity surplus is higher than 3 kW during the day's hottest hours.

Unlike state-of-the-art technologies, small-scale methanation reactors require a reduced complexity of the overall SNG process to keep the specific capital costs reasonable. Simulations by Neubert et al. [45] underlined that a two-stage methanation concept is capable of the production of grid-injectable SNG; thus the following parameters are considered for the methanation reactor under study (Table 4):

Table 4. Methanation reactor characteristics.

Parameter	Value
P_{met}^{Pr}	8 bar
T_{met}	300 °C
F_{CO_2}	0.98

Coupling components efficiency

The efficiency of the coupling process is represented in Figure 14. The electrolyzer hydrogen conversion factor is 4.8 kWh/Nm^3, corresponding to an electrolysis efficiency of 73%. The methanation reactor has an equivalent efficiency of 70%.

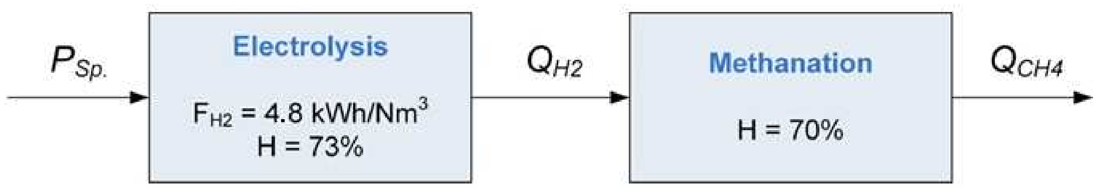

Figure 14. Power-to-gas process.

This means that the overall process efficiency is equal to 51.1%, as expressed by Equation (15).

$$\eta_{tot} = \eta_{electrolysis} \cdot \eta_{methanation} = \frac{Q_{CH_4} \times HHV_{CH_4}}{P_{Sp.}} = 51.1\% \quad (15)$$

where HHV_{CH_4} is the CH_4 higher heating value.

2.7. Scenario Definition

The main scenario configurations are carried out in the following chapters.

2.7.1. Factors Affecting the Simulation Scenarios

Relevant simulation times

Simulations are performed for five relevant time points, as shown in Figure 15. The t_1 = 08:00 h is chosen because, at this time, the gas load is minimal. While t_2 = 10:00 h is chosen because, as is shown in Section 3.2.2, the amount of gas that may be injected into the LP grid is maximal. At t_3 = 11:00 h, the electricity surplus reaches its maximal value. The other two simulation points are chosen to study the gas grid behavior when the SNG production, and thus the injection into the LP pipeline, is stopped. At t_4 = 17:00 h, the gas load increases and peaks at t_5 = 20:00 h.

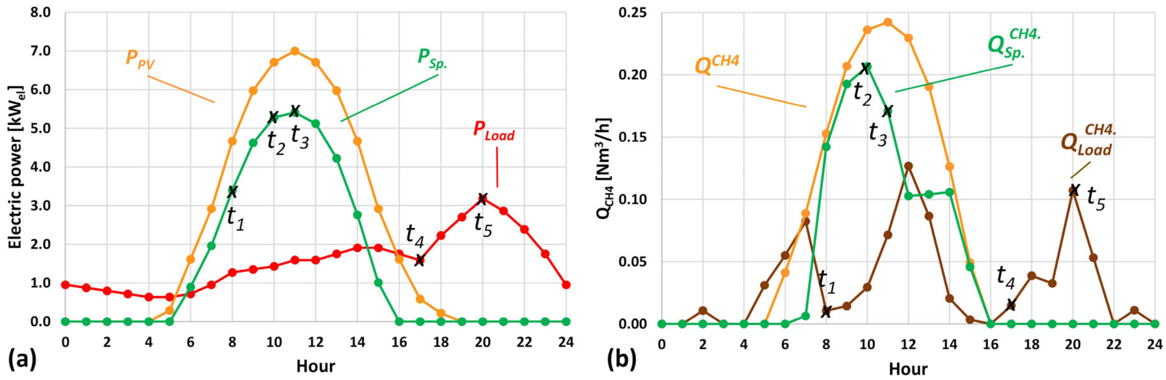

Figure 15. Simulation time points. (**a**) Electricity profiles: P_{PV}, P_{load}, and P_{sp} are, respectively, PV production, electric demand, and PV surplus profiles. (**b**) Gas profiles: Q^{CH4}, Q^{CH4}_{Load}, and $Q^{CH4}_{Sp.}$ are, respectively, SNG production, thermal demand, and SNG surplus profiles.

Slack voltages

An important aspect to consider when analyzing the LV grid is that the input voltage may differ from the nominal value, depending on the DTR's connection point within the MV network. Distributed electricity injection locally increases the voltage even in the MV feeder, so supplying transformers, i.e., MV step-down transformers, which are equipped with the on-line tap changer (OLTC), can impose a voltage value lower than the nominal one at the MV feeder head (FHd).

When the LV grid's connection point is at the MV FHd (point A), voltage may be 2% lower than the nominal as DTRs lack OLTCs. Conversely, a connection at the MV endpoint (point B) may result in up to a 6% voltage increase over the nominal value, as highlighted in Figure 16. This variation affects available thresholds and, if voltage decreases, load also decreases (Equation (A1)), contributing to a higher electricity surplus.

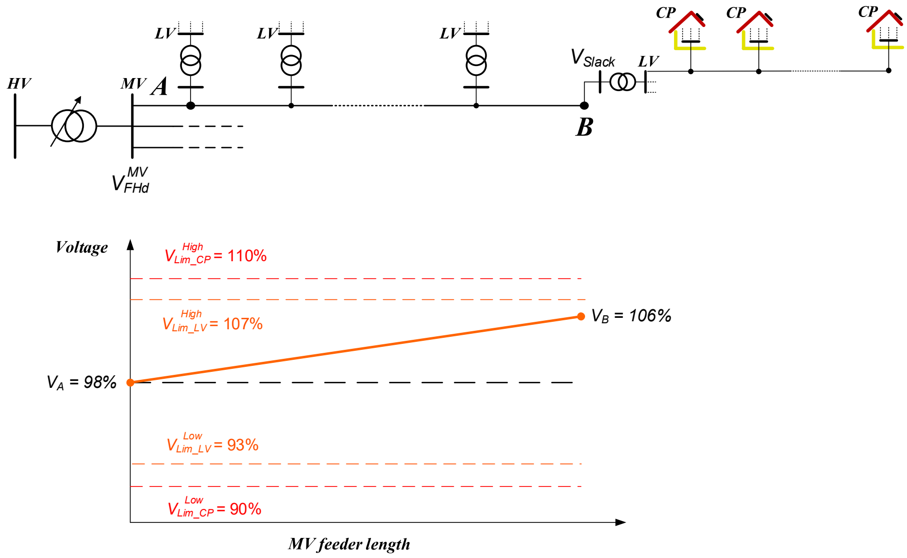

Figure 16. DTR's connection point in MV feeder; V_A = 98%; V_B = 106%.

The setting of nominal pressure downstream of the PRG is more manageable than setting the pressure ratio in the electricity grid as the lamination valve functions by imposing downstream pressure and adjusting its resistance based on upstream pressure. This type of regulation responds to fluid-dynamic aspects and does not require a control scheme or additional costs. So, even if the pressure increases or decreases along the MP pipeline, the available threshold to inject or consume gas without violating the limits is everywhere the same at each hour.

These considerations conclude that two input voltage values must be analyzed, i.e., V = 106% and V = 98%.

Primary LP pipeline diameter size

The primary LP pipeline diameter significantly influences technical limitations within the gas grid and affects the linepack effect; thus, it is the primary variable in this study. The secondary LP pipeline diameter has an essential impact on the linepack effect but not on technical limitations.

Downstream nominal pressure value in the PRG

The nominal pressure downstream of the PRG impacts pipeline storage capacity as higher nominal pressure decreases the linepack effect, as assessed in Appendix C.

2.7.2. Scenario Overview

The scenario overview is shown in Table 5. Firstly, the electricity grid behavior is analyzed for two different slack voltages (V = 98% and V = 106%) for all five simulation times unaffected by gas grid parameters. Then, the analysis of gas grid injections with a nominal pressure of 30 mbar and a primary LP pipeline diameter of 30 mm is carried out. In this case, the chosen electricity grid configuration is V = 98% because the lower the voltage, the higher the electricity and, thus, the gas surplus. Furthermore, these analyses have been repeated for different diameter sizes in the range of 10 ÷ 30 mm in the most critical hour (t_2 = 10.00). Finally, the potential for the linepack effect exploitation was investigated by analyzing the gas grid behavior with the minimum nominal pressure value downstream of the PRG equal to 20 mbar.

Table 5. Scenario overview.

Electricity		Gas	
Simulation Times	**Slack Voltage**	**Diameter Size**	**PRG Pressure**
t_1 = 08:00 h	V = 98% V = 106%	10 ÷ 30 mm	20 ÷ 39 mbar
t_2 = 10:00 h	V = 98% V = 106%	10 ÷ 30 mm	20 ÷ 39 mbar
t_3 = 11:00 h	V = 98% V = 106%	10 ÷ 30 mm	20 ÷ 39 mbar
t_4 = 17:00 h	V = 98% V = 106%	10 ÷ 30 mm	20 ÷ 39 mbar
t_5 = 20:00 h	V = 98% V = 106%	10 ÷ 30 mm	20 ÷ 39 mbar

3. Results and Discussion

3.1. Behavior of the Electricity Grid

If the LV feeder connects at the MV Feeder Head (FHd) with V = 98%, injecting electricity surplus back into the LV grid does not induce voltage issues. However, if the LV feeder connects at the end of the MV line (V = 106%), voltage issues arise despite a higher load (and therefore reduced surplus).

Figure 17 shows the voltage profiles, assuming all buildings have a 7 kW_p PV facility installed on their rooftops. At 17:00 h and 20:00 h, when the PVs do not produce electricity, all customers are supplied by the MV grid. The voltage profile has a descending course; no voltage problems occur. At 08:00 h, the PV production covers the electrical load and produces a surplus of ca. 3.4 kW. The voltage profile has a slightly rising course without provoking any voltage violation. But at 10:00 h and 11:00 h, each CP injects in the grid ca. 5.2 kW, causing a feedback flow to the MV grid of 101 kW. Both voltage profiles have a rising course, causing the violation of the upper voltage limit. In this case, the DSOs must take countermeasures (install OLTC in each DTR or use reactive power control) to alleviate the upper voltage limit violation or prohibit rooftop PV installation in each customer plant.

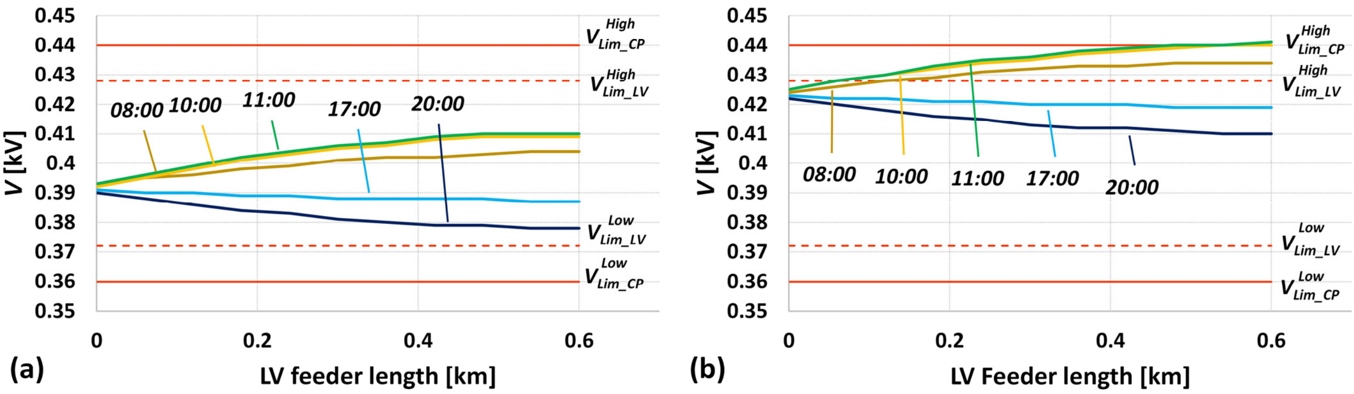

Figure 17. Voltage profiles in LV feeder for different simulation times and different slack voltages. (**a**) V = 98%. (**b**) V = 106%.

3.2. Behavior of the Gas Grid

3.2.1. SNG Production at the Customer Plant Level

Due to the limitations in hosting capacity within the electricity grid, surplus electricity can be used for SNG production, which can partly meet the CP's gas demand and partly be re-injected into the gas grid. Additional power requirements for H_2O compression and CO_2 and H_2 heating result in increased electric and gas loads at each CP, as illustrated in Figure 18:

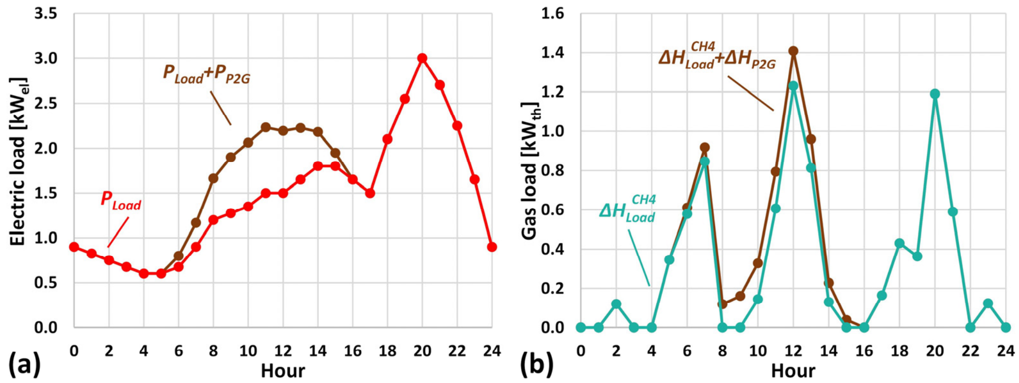

Figure 18. Upgraded load profiles after P2G processes. (**a**) Electric load. (**b**) Gas load.

The efficiency of the process is represented in Figure 19. For instance, a 5 kW surplus from the PV enables H_2 production in an AEM electrolyzer with a conversion rate of 4.8 kWh/Nm^3 and 0.25 Nm^3/h of SNG generated in the methanation reactor. Though, the overall efficiency of the process, as expressed in Section 2.6.2, is 51.1%.

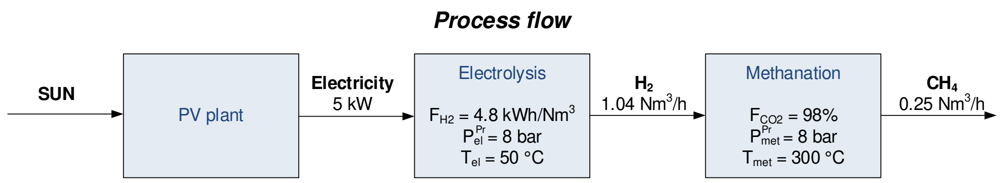

Figure 19. Power-to-gas process.

A daily analysis reveals how SNG production is affected by the voltage at the beginning of the LV feeder, as shown in Figure 20.

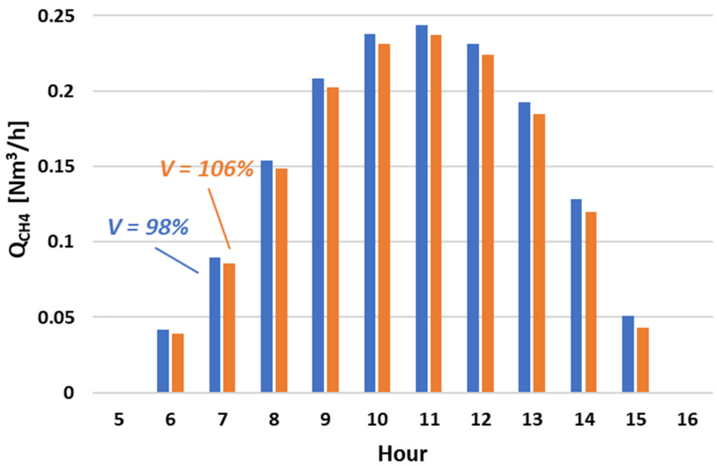

Figure 20. Production of SNG on a typical summer day for two extreme slack voltage values, 98% and 106%, provoked by the connection point of the DTR at the MV feeder.

Figure 20 illustrates that there is electricity surplus only between 06:00 h and 15:00 h. The produced SNG increases when the voltage is lower, driven by a greater surplus from the PV. Specifically, if voltage at the beginning of the LV feeder is lower, the load is also lower (Equation (A1)), resulting in a higher electricity surplus and, consequently, higher SNG production. Therefore, the most critical scenario for gas injections occurs when the LV subsystem is connected at the MV feeder input.

Simulations for the LP gas grid were conducted during these hours and analyzed alongside the LV electricity grid, focusing on the most critical scenario, i.e., when the LV subsystem is connected at the beginning of the MV feeder (Figure 21).

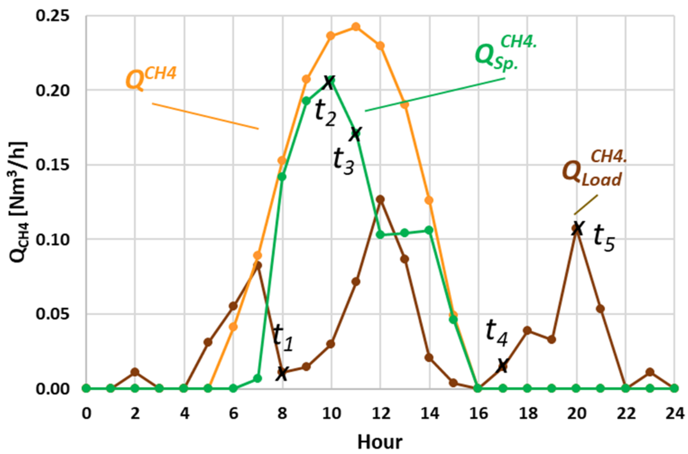

Figure 21. Gas profiles for each CP, V = 98%.

Unlike the pattern observed for injectable electricity, the peak surplus of SNG, amounting to 0.21 Nm^3/h, occurs at 10:00 h. This timing is due to lower consumption during this hour, while production levels remain similar to those observed at 11:00 h.

3.2.2. Injection of SNG Surplus into the Gas Grid

To run LP gas grid simulations, the most essential hypothesis is that a compressor is installed at the PRG to let SNG come back from the LP to the MP grid even if nowadays this component is not installed because it has never been conceived the injection of gas from the end-user and because the valve installed in the PRG is not bidirectional (differently from the DTR in the electricity grid).

So, for V = 98%, the results of a primary LP pipeline diameter of 30 mm, a secondary LP pipeline diameter of 15 mm, and a nominal pressure downstream of the PRG of 30 mbar gas grid are shown in Figure 22.

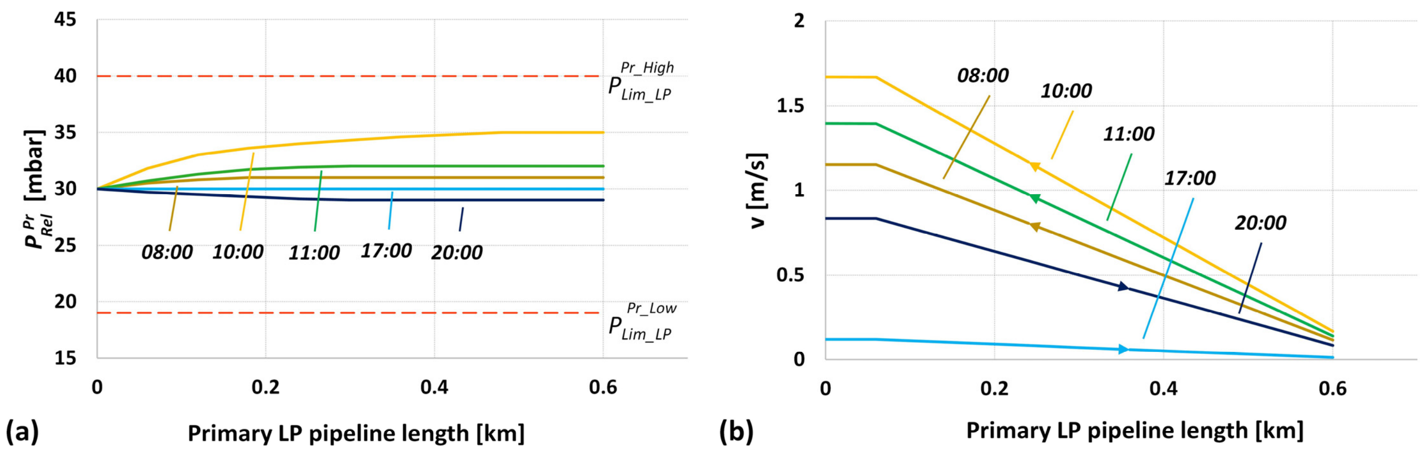

Figure 22. Profiles for a primary LP pipeline diameter of 30 mm, a nominal pressure downstream of the PRG of 30 mbar, and a voltage value at the beginning of the LV feeder of 98%: (**a**) Pressure. (**b**) Velocity.

The PRG is placed at the beginning of the primary LP pipeline, and the first couple of CPs are 0.06 km away. Figure 22 shows that when NG is supplied from the MP grid (during late hours of the day), pressure along the pipeline diminishes when no electricity surplus is available. In contrast, the pressure increases at 8:00 h, 10:00 h, and 11:00 h when SNG is produced and injected back from each CP. Velocity always increases proportionally to the gas flow rate because the diameter is the same along the primary LP pipeline. As the first couple of CPs are 0.06 km away from the PRG, velocity remains the same in the first stretch. Pressure drops are proportional to velocity squared, though pressure parabolically increases (or decreases).

Finally, Figure 22 highlights that, in contrast to electricity grid injections, no pressure issues arise at 10:00 h—when SNG injections are at their maximum—and velocity inside LP pipelines is always lower than the limit of 5 m/s. Thus, no velocity problems happen when assessing the fact that this can be a viable solution to exploit all the benefits offered by the DG.

However, the outcomes for the gas grid are significantly affected by the diameter of the primary LP pipe, as shown in Figure 23.

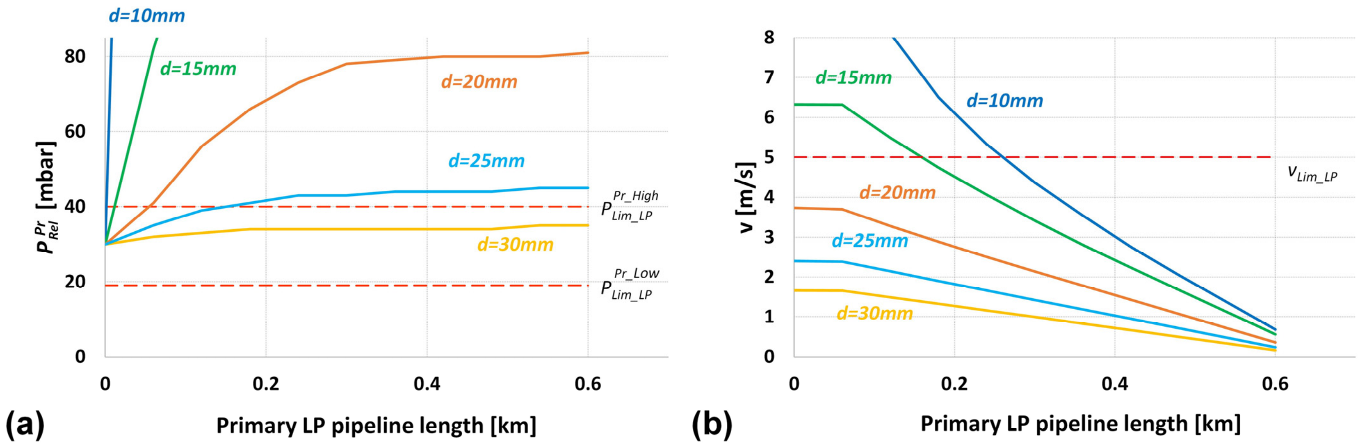

Figure 23. Profiles for multiple primary LP pipeline diameters. Nominal pressure downstream of the PRG of 30 mbar, voltage value at the beginning of the LV feeder of 98%. (**a**) Pressure. (**b**) Velocity.

Figure 23 highlights pressure and velocity profiles inside the primary LP pipeline at 10:00 h, varying the primary LP pipeline diameter size. It shows that the lower the diameter, the higher the velocity and, consequently, the pressure. Pressure strongly increases because the closer SNG gets to the beginning, the higher the SNG flow rate flows through the pipe. Thus, the pressure drop is more significant. Pressure is way more influenced by diameter than velocity, but for d = 15 mm, velocity problems occur, too. Maximum pressure happens at the end of the LP pipeline because a higher thrust is necessary to make SNG flow through the pipe. In contrast, maximum velocity occurs at the beginning of the LP pipeline.

The secondary LP pipeline's diameter's limitations are way lower because the SNG flow rate flowing into them comes from a single CP, so it is always low.

The relationships between maximum pressure and velocity with the primary LP pipe diameter are depicted in Figure 24.

Figure 24 indicates that the maximum allowable pressure constitutes the most critical limitation. Specifically, while a minimum diameter of 18 mm is required to avoid velocity issues, a minimum diameter of 27 mm is necessary to prevent pressure problems. Furthermore, the figure demonstrates that for diameters exceeding 45 mm, pressure remains constant, thus facilitating the effective exploitation of linepack advantages even at higher nominal pressure values. This means that additional costs are requested to exploit the DG advantages, such as in the electricity grid and gas grid, but technical limitations are much inferior.

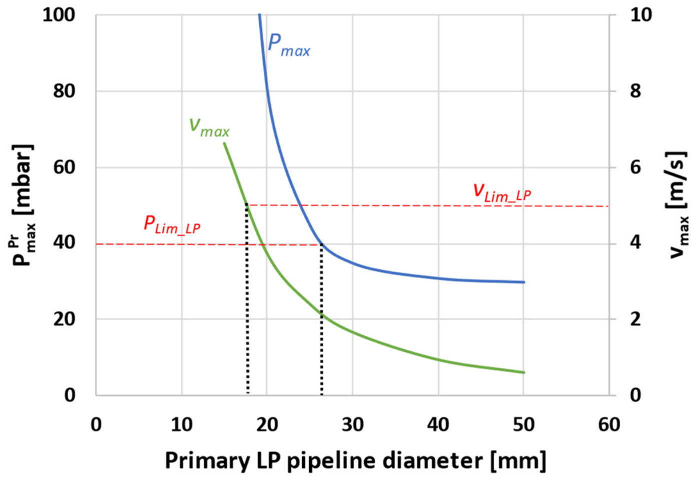

Figure 24. Dependence of maximum pressure and velocity on primary LP pipe diameter.

Finally, if the available electricity surplus is exploited each hour of the day to produce and inject SNG, the following daily results are obtained:

- PV production covers 50% of the daily electric load;
- Daily H_2O used by each CP is just 5 kg, thus not creating H_2O supply problems;
- Daily CO_2 used in the methanation reactor by each CP is almost 3.2 kg, thus creating the possibility to cut emissions, promoting the growth of the CO_2 market;
- SNG production is almost two times the gas load, but because of the non-simultaneous difference between production and consumption, the daily covered thermal load is 60%. Thus, 70% of the daily SNG production from each CP is injected back into the LP grid;
- For all twenty connected CPs, the total SNG to be transferred from LP to MP grid is 21.9 Nm^3.

3.2.3. Linepack Effect

The linepack effect is the possibility of exploiting the storage capability of the pipeline itself, as expressed in Appendix C.

The storage capability is maximized when the nominal pressure downstream of the PRG is 20 mbar (close to the lower limit), and the maximum allowable one is 39 mbar (close to the higher limit). Thus, to exploit the linepack effect, as shown in Figure 24, a primary LP pipe diameter of at least 45 mm is required to prevent pressure threshold violations during peak injection at 10:00 h and peak consumption at 20:00 h.

With a nominal pressure downstream of the PRG of 20 mbar, a primary LP pipe diameter of 300 mm, and a secondary LP pipe diameter of 150 mm, pressure behavior inside the primary LP pipeline is determined by Equations (A5)÷(A7) (Appendix C) and highlighted in Figure 25.

Figure 25 illustrates that at 06:00 h, when SNG production exceeds NG consumption, SNG is injected back into the LP grid, thereby utilizing the linepack effect until a maximum allowable pressure of 39 mbar is achieved. Then, the compressor within the PRG is activated, allowing SNG to be transferred to the MP grid. Once consumption surpasses production again, the linepack effect is leveraged to meet the gas load until the nominal pressure of 20 mbar is restored. From now on, gas supply from the MP to the LP grid at PRG is resumed, enabling the storage of 0.81 Nm^3 of SNG, which covers 13.5% of the overnight load (i.e., from 17:00 h to 06:00 h).

The storage capability of the pipe, as well as the covered night load percentage, are strongly influenced by the primary and secondary LP pipeline diameter size, as highlighted in Figure 26. The secondary LP pipeline diameter is always considered half of the primary one.

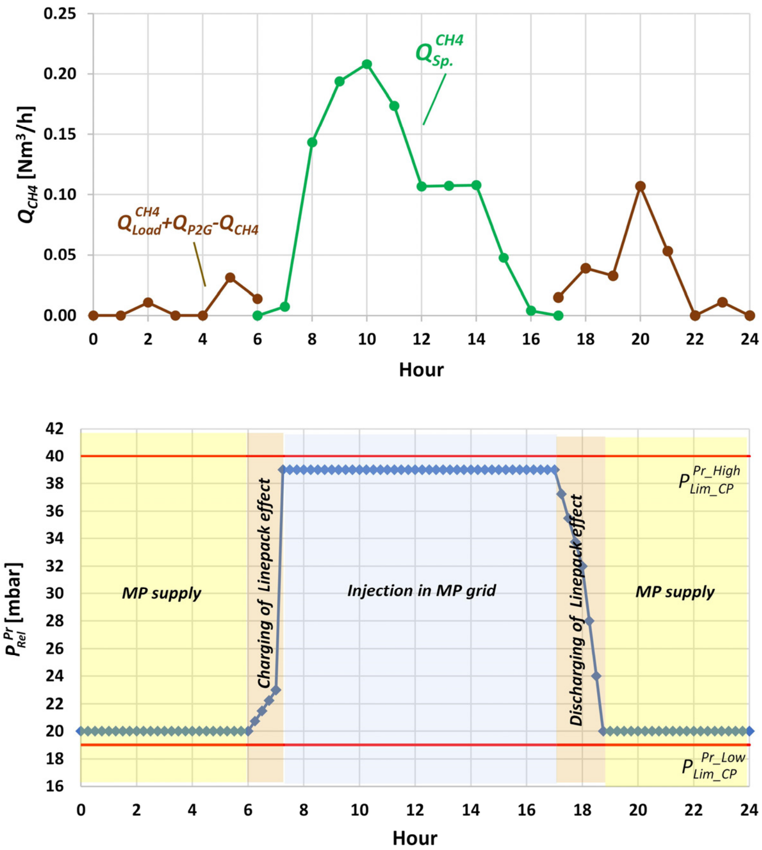

Figure 25. Linepack exploitation: daily pressure profile.

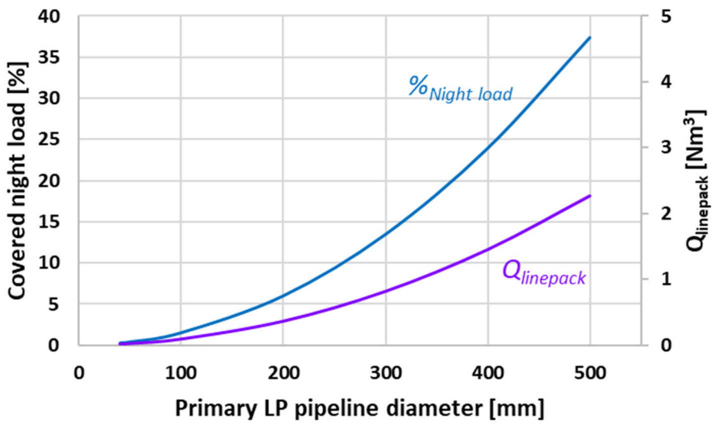

Figure 26. Linepack effect dependency on primary LP pipeline diameter.

The graph starts from a diameter of 45 mm because of the reasons explained at the end of Section 3.2.2. The covered night load percentage increases exponentially with the primary LP pipeline diameter, so the linepack effect is almost negligible up to a diameter value of 80 mm.

3.3. Economic Consideration

Usually, all technical solutions in the energy area have been accompanied by an economic analysis to check their feasibility and guarantee supply affordability for all customers. However, dealing with technical energy issues changed radically in 2015 when the energy trilemma was introduced [50]. Figure 27 shows the energy trilemma with its three equal priorities—energy security, sustainability, and equity—for social stability and environmental sustainability. Balancing this trilemma is difficult and time consuming, if only because of the mutual exclusivity of priorities, and was therefore not the subject of this work.

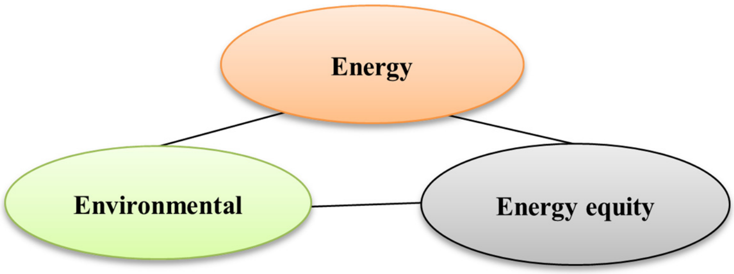

Figure 27. Energy trilemma triangle.

The authors have deliberately refrained from the economic assessment of the proposed solution because it would not meet the requirements of the time. An isolated economic assessment could not consider the solution's significant impact in increasing the security of supply and environmental sustainability by increasing the share of renewable energy resources and the further utilization of the existing infrastructure.

4. Conclusions

The *LINK* framework is essential, as it promotes a unified approach across all levels within both electrical and gas networks. This similarity helps to make the consumers protagonists of the fight against climate change by making them prosumers of electricity and gas. However, voltage issues often limit the benefits of distributed electricity generation when surplus electricity is injected back into higher-voltage grids. To address this, sector coupling, built on the *LINK* architecture, provides an effective solution by coupling electricity and gas grids at various voltage levels, particularly overcoming rooftop photovoltaic integration challenges at the customer plant level.

Results show that an electrolyzer set up at the customer plant level can be supplemented with a methanation reactor to produce synthetic natural gas. The latter will cover the momentary thermal load, and the surplus will be injected into the low-pressure grid. In this way, customer plants transform into gas prosumers. In the studied scenario, the minimum diameter for primary low-pressure pipes, set at 27 mm, posed no significant constraints. For broader applications, every pressure reduction group would require compressor upgrades to facilitate two-way gas flow.

The linepack effect can be effectively exploited, allowing evening thermal loads to be met without requiring expensive storage tanks at each plant. The storage capacity strongly depends on pipeline diameter and length, helping to mitigate the mismatch between energy production and consumption while minimizing compressor use, activated when the pressure inside the low-pressure pipe reaches the maximum allowable value.

Economically, investments at the CP level for electrolysis and methanation systems are necessary. Furthermore, upgrading gas grids with compressors to allow gas to flow from low- to medium-pressure networks involves additional costs.

In the summer, when the electricity and synthetic natural gas production exceeds electrical and gas demand, it may be possible to fill the underground gas storages so that, at least for some time, gas no longer needs to be imported from abroad. Additionally, the stored synthetic natural gas may be used without hesitation to run the gas turbines, which are crucial for the flexibility and security of supply in the presence of highly volatile resources.

Because CO_2 is needed to run the methanation process, a CO_2 market could be developed, encouraging big power plants to adopt carbon capture. Therefore, the emissions will be cut not only from the end-user level but even from the production level.

The feasibility assessment of the proposed solution will be subject to further work considering the energy trilemma, thus it will involve a year-long analysis to evaluate the effects of seasonality on the economic feasibility of the solution. Additionally, possible safety scenarios will be analyzed, as hydrogen systems pose risks that have discouraged their widespread use in some sectors.

Author Contributions: Conceptualization A.I. and A.A.; methodology A.I., C.C. and A.A.; validation C.C. and A.I.; formal analysis A.A.; investigation A.A.; writing—original draft preparation A.A.; writing—review and editing, A.I. and C.C.; supervision A.I. and C.C. Informed consent was obtained from all subjects involved in the study. All authors have read and agreed to the published version of the manuscript.

Funding: This paper is written based on the cooperation between the "Dipartimento di Ingegneria Industriale, Università degli studi di Firenze, Italy" and "Institute of Energy Systems and Electrical Drives, TU Wien, Austria". A.A. wrote his master's thesis, which forms the basis of this paper, at the TU Wien, funded by the Erasmus+Traineeship EU's program.

Institutional Review Board Statement: Not applicable.

Informed Consent Statement: Not applicable.

Data Availability Statement: Data are contained within the article.

Conflicts of Interest: The authors declare no conflicts of interest.

Abbreviations

Acronyms

CC	Coupling component
CNG	Compressed natural gas
Cook	Gas cooker
CP	Customer plant
Dev.	Device
DG	Distributed generation
DH	District heating
DHW	Domestic hot water
DER	Distributed energy resources
DSO	Distribution system operators
DTR	Distribution transformer
E-St.	Electric storage
EU	European Union
FHd	Feeder head
G-St.	Gas storage
HHV	Higher heating value
HP	High pressure
HV	High voltage
LNG	Liquified natural gas
LP	Low pressure
LV	Low voltage
MP	Medium pressure
MV	Medium voltage
NG	Natural gas
OLTC	On-load tap changer
P2G	Power-to-gas
P2P	Power-to-power
PP	Power plant
Pr.	Producer
PRG	Pressure reduction group
PV	Photovoltaic
SC	Sector coupling
SNG	Synthetic natural gas
TSO	Transmission system operator

Symbols

Electricity grid symbols	
$\cos\varphi$	Power factor (-)
f_n	Rated frequency (Hz)
C	Zip coefficient (-)
I	Current (A)
l	Line length (km)
P_{PV}	PV production power (kW)
P_{Load}	Electric load power consumption (kW)
$P_{Sp.}$	Surplus electric power (kW)
P_{P2G}	P2G electric load power (kW)
$P_{Sp.}^{CH4}$	Surplus electric power to produce SNG (kW)
q	Line cross-section (mm^2)
Q	Reactive power (kVAR)
S_n	Rated apparent power (kVA)
V	Voltage percentage compared to nominal voltage value (%)
V_{n1}	Rated voltage side 1 (kV)
V_{n2}	Rated voltage side 2 (kV)
V_{nom}	Rated voltage (kV)
$V_{Lim\_LV}^{High}$	Low-voltage grid higher-voltage limit (V)
$V_{Lim\_LV}^{Low}$	Low-voltage grid lower-voltage limit (V)
$V_{Lim\_CP}^{High}$	Customer plant higher-voltage limit (V)
$V_{Lim\_CP}^{Low}$	Customer plant lower-voltage limit (V)
V_{FHd}^{MV}	Voltage value at MV feeder head
Z	Impedance (Ω)
Gas grid symbols	
d	Pipe diameter (mm)
ΔH	Thermal power (kW)
ΔH^{Peak}	Peak thermal power (kW)
ΔH_{Load}^{CH4}	Gas load power consumption (kW)
ΔH_{P2G}	P2G gas load power (kW)
$\Delta H_{Sp.}^{CH4}$	Surplus gas power (kW)
H	Elevation (m)
l	Pipe length (m)
m^{mass}	Mass of gas (kg)
$m_{inj\_tot}^{mass}$	Total injectable mass of gas (kg)
m_{inj}^{mass}	Injectable mass of gas from each CP (kg)
mol	Number of moles of a chemical substance (mol/h)
Mw	Molecular weight of a chemical substance (g/mol)
N_{CPs}	Number of connected customer plants (-)
P^{Pr}	Absolute pressure (Pa)
P_{rel}^{Pr}	Relative pressure (Pa)
P_n^{Pr}	Normal pressure (Pa)
$P_{Lim\_LP}^{\mathrm{Pr}\_High}$	Low-pressure grid higher-relative pressure limit (Pa)
$P_{Lim\_LP}^{\mathrm{Pr}\_Low}$	Low-pressure grid lower-relative pressure limit (Pa)
Q	Normal volumetric flow rate (Nm^3/h)
R	Gas constant (J/kgK)
R_s	Sand roughness (mm)
T_n	Normal temperature (K)
T	Gas temperature (K)
Vol	Volume (m^3)
v_{max}	Maximum velocity (m/s)
Z	Gas compressibility factor (-)
ρ	Density (kg/m^3)
Coupling components symbols	
c_p	Specific heat at constant pressure (J/kgK)
ΔH_{H_2}	Thermal power requested to heat H_2 (kW)

ΔH_{CO_2}	Thermal power requested to heat CO_2 (kW)
F_{H_2}	H_2 Conversion rate (kWh/Nm^3)
F_{CO_2}	CO_2 Conversion efficiency factor (-)
P_{el}^{Pr}	Absolute pressure of the electrolyzer (Pa)
P_{met}^{Pr}	Absolute pressure of the methanation reactor (Pa)
T_{el}	Temperature of the electrolyzer (K)
T_{met}	Temperature of the methanation reactor (K)
T_{tank}	Temperature inside the tank (K)
η_{pump}	Pump efficiency (-)
η_{Gen}	Generator efficiency (-)
η_{boiler}	Boiler efficiency (-)

Appendix A. Electricity and Gas Grid Symbols

Table A1. Symbols used for electrical and gas grids.

Electricity Grid			Gas Grid		
Element	**Symbol**	**Description**	**Element**	**Symbol**	**Description**
Bus bar		Conductor linking multiple circuits	Node		Pipelines' connection point
Line overhead		Overhead feeder for electricity distribution	Pipeline overhead		Overhead pipeline
Line underground		Underground feeder for electricity distribution	Pipeline underground		Underground pipeline
Producer	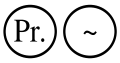	Electric power plant	Gas well	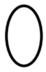	Gas production well
Transformer	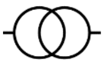	Device that transforms an AC input voltage into a higher or lower AC output voltage	Compressor/ lamination valve	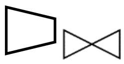	Engine that increases (compressor) or reduces (lamination valve) gas pressure
Storage	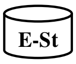	Device designed to store energy generated at one point in time for use when demand is higher	Storage		Device designed to store energy generated at one point in time for use when demand is higher
Load	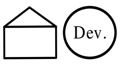	Electrical device or circuit element responsible for consuming electric power	Load	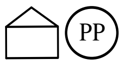	Natural gas consumer
Circuit braker/fuse		Electrical device designed to interrupt the flux of current	Non-return valve		Component used to interrupt the flux of gas in one direction

Appendix B. Electricity Grid Modeling

Regarding the electricity grid, the electric load modeling and the voltage limits description are highlighted below.

Electric load dependency from the voltage

The power consumption of the electrical loads depends significantly on the voltage value. Considering this dependency is essential to perform accurate power flow calculations in low-voltage grids. The polynomial expression known as the ZIP coefficients [51] model represents the load's variation (with voltage) as a composition of the three types of constant loads: constant impedance Z; constant current I; and constant power P. The expressions for active and reactive powers of the ZIP coefficients model are:

$$P_i = P_0\left(C_{P,P} + C_{I,P}\frac{V_i}{V_n} + C_{Z,P}\left(\frac{V_i}{V_n}\right)^2\right) \quad \text{(A1)}$$

$$Q_i = Q_0\left(C_{P,Q} + C_{I,Q}\frac{V_i}{V_n} + C_{Z,Q}\left(\frac{V_i}{V_n}\right)^2\right) \quad \text{(A2)}$$

where P_i and Q_i are the active and reactive powers at operating voltage V_i; P_0 and Q_0 are the active and reactive powers at nominal voltage V_n; $C_{Z,P}$, $C_{I,P}$, and $C_{P,P}$ are the ZIP coefficients for active power; $C_{Z,Q}$, $C_{I,Q}$, and $C_{P,Q}$ are the ZIP coefficients for reactive power.

ZIP coefficients satisfy the following constraints:

$$C_{P,P} + C_{I,P} + C_{Z,P} = 1 \quad \text{(A3)}$$

$$C_{P,Q} + C_{I,Q} + C_{C,Q} = 1 \quad \text{(A4)}$$

Voltage limits

It is essential that devices in CPs receive a well-defined voltage level regardless of whether they are consuming or injecting electricity, as deviations could lead to damage. Accordingly, the grid must supply electricity within a maximum threshold of ±10% of the nominal value.

An even stricter limitation applies within each CP, where an additional local grid connects all devices (see Figure A1).

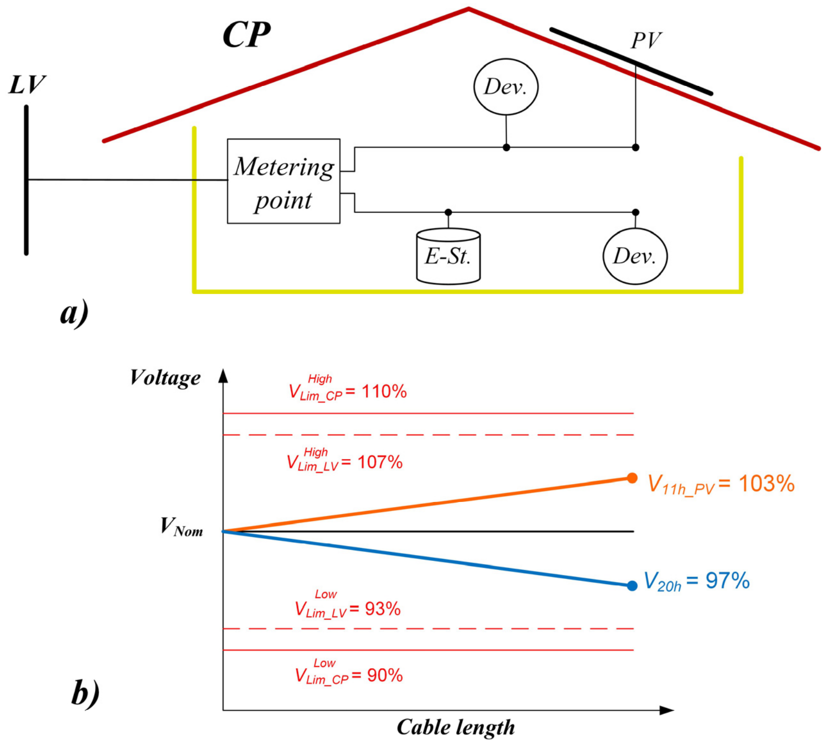

Figure A1. Determination of voltage limits in low-voltage grid. (**a**) CP grid. (**b**) CP and LV grid voltage limits [52].

The figure shows that the last connected device can suffer another voltage variation of about ±3% depending on whether it injects or consumes electricity. In the first case, the voltage rises because a higher electricity injection brings higher voltage drops along the cable. In contrast, in the second case, a higher electricity consumption brings higher voltage drops along the cable in the opposite direction. In both cases, voltage drops have a linear behavior along the cable. For this reason, the maximum allowable voltage threshold of the low-voltage (LV) grid becomes ±7% of the nominal value.

Electricity grid parameters

Table A2. Electricity grid's input data.

Component	Input Data	Symbol	Value
Slack	Voltage percentage	V	Scenario: 98 ÷ 106%
Two-winding transformer	Rated voltage side 1 Rated voltage side 2 Rated apparent power	V_{n1} V_{n2} S_n	10 kV 0.4 kV 250 kVA
Primary LV feeder	Total length Cross-section	l q	600 m 150 mm^2
Secondary LV feeders	Total length Cross-section	l q	200 m 50 mm^2
Load	Active power Reactive power P, Q constant I constant Z constant Load electricity profile	P_{Load}^{Peak} Q_{Load} $C_{P,P}$; $C_{P,Q}$ $C_{I,P}$; $C_{I,Q}$ $C_{Z,P}$; $C_{Z,Q}$ -	3 kW 1 kVAR 0.96; 6.28 −1.17; −10.16 1.21; 4.88 Residential
PV	Rated voltage Active power Power factor	V P_{PV}^{Peak} $\cos\varphi$	0.4 kV 7 kW 1

The voltage percentage value depends on the analyzed scenario (Section 2.7.1). The profiles used for the simulation have been imposed as input data in the load (residential profile) and in the PV (PV profile) to run daily simulations.

Modeling of grid components

The line and transformer models are shown in the following [53].

Line modeling

The following equivalent circuit diagram simulates lines in the positive-phase sequence, Figure A2.

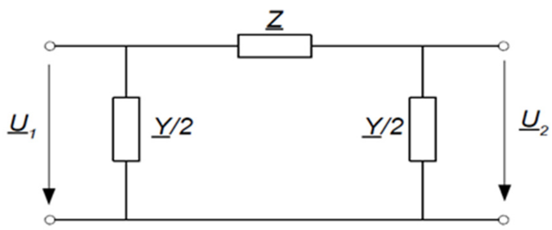

Figure A2. Equivalent π circuit diagram of the line.

Transformer modeling

The following equivalent circuit diagram characterizes the uncontrolled distribution transformer (none OLTC), Figure A3.

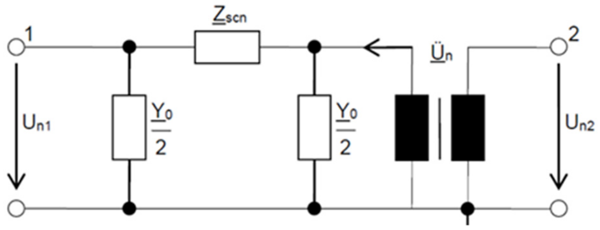

Figure A3. Equivalent circuit diagram of the transformer.

Appendix C. Gas Grid Modeling

Regarding the gas grid, the pressure limits description, the linepack effect, and the gas grid components modeling are highlighted below.

Pressure limits

Appliances in CPs also require a defined pressure level close to atmospheric pressure; excessively high pressure poses an explosion risk, whereas excessively low pressure may prevent adequate supply due to insufficient gas flow driving force. Currently, if relative pressure in LP pipelines drops below 19 mbar, safety protocols immediately shut off gas flow to appliances, such as boilers and cookers. Thus, the LP grid must provide gas without exceeding the upper limit of 40 mbar and the lower one of 19 mbar (Figure A4).

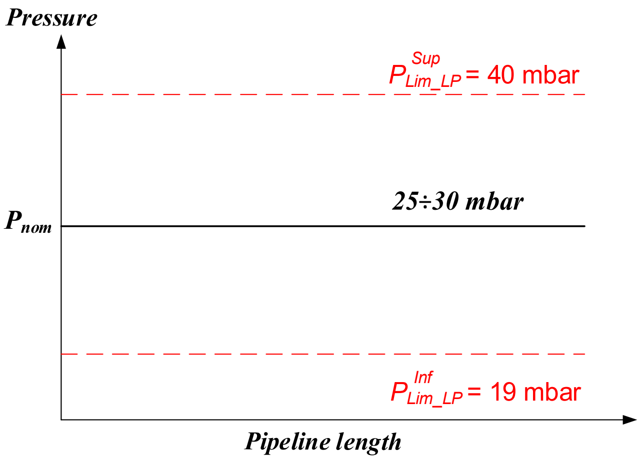

Figure A4. LP grid pressure limits [54].

Linepack effect

Pipelines can act as storage systems for compressible gas, known as the linepack effect, due to their specific diameter and gas-hosting capability. Pressure variations are not instantaneous because the pipeline's capability is high and because convective and diffusive phenomena, the driving fluid dynamic ones, have a particular characteristic time.

Thanks to this unsteady behavior and wide pressure limits, pressure regulating valves in pressure reduction groups (PRGs) have a high grade of flexibility, and security constraints may be easily respected compared with the electricity grid case, where voltage limits are more restrictive.

So, the storage capability of the pipeline is higher if the downstream nominal pressure value in PRGs is lower. The maximum storage capability is achieved once the pressure inside the pipeline reaches the maximum allowable value (40 mbar).

Thus, the maximum mass of gas injectable from each CP (m_{inj}^{mass}) can be found using Equation (A7).

$$m_{in}^{mass} = \frac{P_{in}^{Pr}}{Z \times R \times T} \times Vol \tag{A5}$$

$$m_{fin}^{mass} = \frac{P_{fin}^{Pr}}{Z \times R \times T} \times Vol \tag{A6}$$

$$m_{inj}^{mass} = \frac{m_{fin}^{mass} - m_{in}^{mass}}{N_{CPs}} \quad \text{(A7)}$$

where Vol, P_{in}^{Pr}, P_{fin}^{Pr}, m_{in}^{mass}, m_{fin}^{mass}, Z, R, T, and N_{CPs} represent the volume of pipelines (m^3), initial and final pressure (Pa), initial and final mass of gas in the pipelines (kg), compressibility factor (-), specific gas constant (J/kgK), temperature (K), and the total count of connected CPs (-).

Gas grid modeling

The simulated gas grid is composed of the following elements whose parameters have been chosen following the state-of-the-art of a general LP grid. The input data for each component belonging to the gas grid are shown in Table A3.

Table A3. Gas grid parameters.

Component	Input Data	Symbol	Value
Pressure supply	Constant excess pressure	P_{nom}^{Pr}	Scenario: 0.020 ÷ 0.039 bar
Node	Elevation	H	0 m
Primary LP pipeline	Total length Diameter Sand roughness	l d Rs	600 m Scenario: 15 ÷ 300 mm 1.25 mm
Secondary LP pipelines	Total length Diameter Sand roughness	l d Rs	200 m Scenario: 7.5 ÷ 150 mm 1.25 mm
Consumer	Consumption type Constant consumption Time series	- Q -	Standard Q_{CH_4} consumed Nm^3/h Thermal profile
Flow supply	Flow supply type Constant supply Time series	- Q -	Standard Q_{CH_4} produced Nm^3/h SNG injection profile

References

1. ETIP SNET. Smart Sector Integration, Towards an EU System of Systems: Building Blocks, Enablers, Architectures, Regulatory Barriers, Economic Assessment. April 2021, p. 95. Available online: https://www.etip-snet.eu/about/etip-snet/ (accessed on 15 September 2023).
2. Lund, H.; Østergaard, P.A.; Connolly, D.; Mathiesen, B.V. Smart energy and smart energy systems. *Energy* **2017**, *137*, 556–565. [CrossRef]
3. Vaziri, M.; Vadhva, S.; Oneal, T.; Johnson, M. Distributed generation issues, and standards. In Proceedings of the 2011 IEEE International Conference on Information Reuse & Integration, Las Vegas, NV, USA, 3–5 August 2011. [CrossRef]
4. Bertani, A.; Borghetti, A.; Bossi, C.; De Biase, L.; Lamquet, O.; Massucco, S.; Morini, A.; Nucci, C.A.; Paolone, M.; Quaia, S.; et al. Management of Low Voltage Grids with High Penetration of Distributed Generation: Concepts, implementations and experiments. In Proceedings of the CIGRE 2006 Session, Paris, France, 27 August–1 September 2006; pp. 1–6.
5. Witzmann, R.; Esslinger, P.; Norbert, G.; Sebastian, G.; Reinhold, K.; Anita, A. Improving power quality and capacity in low-voltage grids with decentral power generation using intelligent inverters. In Proceedings of the International ETG Congress, Würzburg, Germany, 8–9 November 2011; pp. 8–9.
6. Taljan, G.; Krasnitzer, M.; Strempfl, F.; Jarz, A. Spannungsniveau im 30-kV Netz UW Judenburg/West Lösungsansätze mit Smart Grids. In Proceedings of the Symposium Energieinnovation, Graz, Austria, 15–17 February 2012; pp. 15–17.
7. Procházka, K.; Kysnar, F.; Mezera, D.; Vaculík, P.; Novotny, J. Voltage quality and reactive power flow solution in distribution networks with a high share of renewable energy sources. In Proceedings of the CIRED, Stockholm, Sweden, 10–13 June 2013; pp. 1–5.
8. Elbs, C. Netzeinsparungsmöglichkeiten und Erfahrungen Einer Realen Q(U)-Einführung bei PV Wechselrichtern im Bundesland. Smart Grid Week. 2014, pp. 19–23. Available online: https://nachhaltigwirtschaften.at/resources/edz_pdf/events/20140523_sgw14_vortrag_02_elbs.pdf?m=1646753469& (accessed on 22 December 2023).
9. Turitsyn, K.; Sulc, P.; Backhaus, S.; Chertkov, M. Options for control of reactive power by distributed photovoltaic generators. *Proc. IEEE* **2011**, *99*, 1063–1073. [CrossRef]

10. Malekpour, A.R.; Pahwa, A. Reactive power and voltage control in distribution systems with photovoltaic generation. In Proceedings of the 2012 North American Power Symposium, NAPS 2012, Champaign, IL, USA, 9–11 September 2012; pp. 1–6. [CrossRef]
11. Bolognani, S.; Zampieri, S. A Distributed control strategy for reactive power compensation in smart microgrids. *IEEE Trans. Autom. Control* **2013**, *58*, 2818–2833. [CrossRef]
12. Ilo, A.; Bruckner, H.; Olofsgard, M.; Adamcova, M.; Werner, A. Viable Fully Integrated Energy Community Based on the Holistic *LINK* Approach. *Energies* **2023**, *16*, 2935. [CrossRef]
13. Pastore, L.M.; Sforzini, M.; Basso, G.L.; de Santoli, L. H2NG environmental-energy-economic effects in hybrid energy systems for building refurbishment in future National Power to Gas scenarios. *Int. J. Hydrogen Energy* **2022**, *47*, 11289–11301. [CrossRef]
14. Cavana, M.; Mazza, A.; Chicco, G.; Leone, P. Electrical and gas networks coupling through hydrogen blending under increasing distributed photovoltaic generation. *Appl. Energy* **2021**, *290*, 116764. [CrossRef]
15. Deymi-Dashtebayaz, M.; Ebrahimi-Moghadam, A.; Pishbin, S.I.; Pourramezan, M. Investigating the effect of hydrogen injection on natural gas thermo-physical properties with various compositions. *Energy* **2019**, *167*, 235–245. [CrossRef]
16. Guzzo, G.; Cheli, L.; Carcasci, C. Hydrogen blending in the Italian scenario: Effects on a real distribution network considering natural gas origin. *J. Clean. Prod.* **2022**, *379*, 134682. [CrossRef]
17. Lubello, P.; Pasqui, M.; Mati, A.; Carcasci, C. Assessment of hydrogen-based long term electrical energy storage in residential energy systems. *Smart Energy* **2022**, *8*, 100088. [CrossRef]
18. Mati, A.; Ademollo, A.; Carcasci, C. Assessment of paper industry decarbonisation potential via hydrogen in a multi-energy system scenario: A case study. *Smart Energy* **2023**, *11*, 100114. [CrossRef]
19. Ademollo, A.; Mati, A.; Pagliai, M.; Carcasci, C. Exploring the role of hydrogen in decarbonising energy-intensive industries: A techno-economic analysis of a solid oxide fuel cell cogeneration system. *J. Clean. Prod.* **2024**, *469*, 143254. [CrossRef]
20. Thema, M.; Bauer, F.; Sterner, M. Power-to-Gas: Electrolysis and methanation status review. *Renew. Sustain. Energy Rev.* **2019**, *112*, 775–787. [CrossRef]
21. Methanation of CO_2 to CH_4 Using H_2 Through Sabatier Reaction: A Comprehensive Technical Guide. Available online: https://www.hydrogennewsletter.com/methanation-of-co2-to-ch4-using-h2-through-sabatier-reaction/ (accessed on 13 May 2024).
22. Becker, W.L.; Penev, M.; Braun, R.J. Production of synthetic natural gas from carbon dioxide and renewably generated hydrogen: A techno-economic analysis of a power-to-gas strategy. *J. Energy Resour. Technol. Trans. ASME* **2019**, *141*, 021901. [CrossRef]
23. Tang, Z.; Zhang, L.; Gao, R.; Wang, L.; Li, X.; Zhang, C. Efficient Utilisation of Carbon Dioxide in Power-to-Gas and Power-to-Liquid Processes: A Vital Path to Carbon Neutrality. *Processes* **2023**, *11*, 1898. [CrossRef]
24. Quarton, C.J.; Samsatli, S. Power-to-gas for injection into the gas grid: What can we learn from real-life projects, economic assessments and systems modelling? *Renew. Sustain. Energy Rev.* **2018**, *98*, 302–316. [CrossRef]
25. He, G.-X.; Yan, H.-G.; Chen, L.; Tao, W.-Q. Economic dispatch analysis of regional Electricity–Gas system integrated with distributed gas injection. *Energy* **2020**, *201*, 117512. [CrossRef]
26. Held, M.; Schollenberger, D.; Sauerschell, S.; Bajohr, S.; Kolb, T. Power-to-Gas: CO_2 Methanation Concepts for SNG Production at the Engler-Bunte-Institut. *Chem. Ing. Tech.* **2020**, *92*, 595–602. [CrossRef]
27. Giglio, E.; Lanzini, A.; Santarelli, M.; Leone, P. Synthetic natural gas via integrated high-temperature electrolysis and methanation: Part I—Energy performance. *J. Energy Storage* **2015**, *1*, 22–37. [CrossRef]
28. Estermann, T.; Newborough, M.; Sterner, M. Power-to-gas systems for absorbing excess solar power in electricity distribution networks. *Int. J. Hydrogen Energy* **2016**, *41*, 13950–13959. [CrossRef]
29. Ilo, A. Use cases in sector coupling as part of the LINK-based holistic architecture to increase the grid flexibility. *CIRED Open Access Proc. J.* **2020**, *2020*, 529–532. [CrossRef]
30. Ilo, A.; Schultis, D.-L. *A Holistic Solution for Smart Grids based on LINK—Paradigm*; Springer: Berlin/Heidelberg, Germany, 2022.
31. Rosenberg, M. The 5 Sectors of the Economy. ThoughtCo. 2020. Available online: https://www.thoughtco.com/sectors-of-the-economy-1435795 (accessed on 8 June 2024).
32. O'Malley, M.; Kroposki, B.; Hannegan, B.; Madsen, H.; Andersson, M.; D'haeseleer, W.; McGranaghan, M.F.; Dent, C.; Strbac, G.; Baskaran, S.; et al. Energy Systems Integration: Defining and Describing the Value Proposition. Technical Report NREL/TP-5D00-66616. June 2016; p. 9. Available online: http://www.osti.gov/servlets/purl/1257674/ (accessed on 10 June 2024).
33. Van Nuffel, L.; Dedecca, J.G.; Smit, T.; Rade-maekers, K. *Sector Coupling: How Can It Be Enhanced in the EU to Foster Grid Stability and Decarbonise?* Research and Energy; European Parliament: Strasbourg, France, November 2018.
34. European Commission; Bernstrauch, O.; Herce, C. Coupling of Heating/Cooling and Electricity Sectors in a Renewable Energy-Driven Europe. 2022. Available online: https://op.europa.eu/en/publication-detail/-/publication/919a8405-6ed7-11ed-9887-01aa75ed71a1/language-en (accessed on 18 July 2024).
35. Shahidehpour, M.; Fu, Y.; Wiedman, T. Impact of Natural Gas Infrastructure on Electric Power Systems. *Proc. IEEE* **2005**, *93*, 1042–1056. [CrossRef]
36. Li, Q.; An, S.; Gedra, T. Solving natural gas load flow problems using electric load flow techniques. In Proceedings of the North American Power Symposium, Lemnos, Greece, 31 August–3 September 2003; p. 7.
37. Germany: KfW Subsidises over 10,000 Solar Battery Systems—PV Magazine International. Available online: https://www.pv-magazine.com/2015/05/12/germany-kfw-subsidizes-over-10000-solar-battery-systems_100019424/ (accessed on 13 May 2024).

38. Scamman, D.; Newborough, M.; Bustamante, H. Hybrid hydrogen-battery systems for renewable off-grid telecom power. *Int. J. Hydrogen Energy* **2015**, *40*, 13876–13887. [CrossRef]
39. Ademollo, A.; Ilo, A.; Carcasci, C. End-use sector coupling to turn customer plants into prosumers of electricity and gaS. *IET Conf. Proc.* **2023**, *2023*, 357–361. [CrossRef]
40. Li, H.; Niu, R.; Li, W.; Lu, H.; Cairney, J.; Chen, Y.-S. Hydrogen in pipeline steels: Recent advances in characterization and embrittlement mitigation. *J. Nat. Gas Sci. Eng.* **2022**, *105*, 104709. [CrossRef]
41. Blending Hydrogen into the EU Gas System—European Commission. Available online: https://joint-research-centre.ec.europa.eu/jrc-news-and-updates/blending-hydrogen-eu-gas-system-2022-01-19_en (accessed on 13 May 2024).
42. L'Italia Sperimenta L'immissione di Idrogeno Nella Rete Gas. Available online: https://www.h2it.it/litalia-sperimenta-limmissione-di-idrogeno-nella-rete-gas/ (accessed on 13 May 2024).
43. Bünger, U.; Landinger, H.; Pschorr-Schoberer, E.; Schmidt, P.; Weindorf, W.; Jöhrens, J.; Lambrecht, U.; Naumann, K.; Lischke, A. *Power-to-Gas (PtG) in Transport—Current Status and Development Perspectives*; German Aerospace Centre (DLR), Institute for Energy and Environmental Research GmbH (ifeu), Ludwig-Bölkow-Systemtechnik GmbH (LBST), German Biomass Research Centre gGmbH (DBFZ): Munich, Germany; Heidelberg, Germany; Leipzig, Germany; Berlin, Germany, 2014.
44. PSS®SINCAL Power System Planning and Analysis Software—Siemens Global. Available online: https://www.siemens.com/global/en/products/energy/grid-software/planning/pss-software/pss-sincal.html (accessed on 13 May 2024).
45. Neubert, M.; Widzgowski, J.; Rönsch, S.; Treiber, P.; Dillig, M.; Karl, J. Simulation-Based Evaluation of a Two-Stage Small-Scale Methanation Unit for Decentralized Applications. *Energy Fuels* **2017**, *31*, 2076–2086. [CrossRef]
46. Carbon Dioxide | Gases | Airgas. Available online: https://www.airgas.com/Gases/Carbon-Dioxide/category/605 (accessed on 13 May 2024).
47. Carbon Dioxide (CO_2) Supplier | Liquid & Compressed | Linde. Available online: https://www.lindeus.com/gases/buy-liquid-or-compressed-carbon-dioxide-gas (accessed on 13 May 2024).
48. Schaaf, T.; Grünig, J.; Schuster, M.R.; Rothenfluh, T.; Orth, A. Methanation of CO_2—Storage of renewable energy in a gas distribution system. *Energy Sustain. Soc.* **2014**, *4*, 1–14. [CrossRef]
49. Enapter. AEM Electrolyser EL 4.0. Available online: www.enapter.com/aem-electrolyser (accessed on 9 November 2022).
50. Mondial, L.C.D.E.; Partner, P.; Wyman, O. World Energy Council World Energy Trilemma Priority Actions on Climate Change and How to Balance the Trilemma. 2015. Available online: www.worldenergy.org (accessed on 12 July 2024).
51. Bokhari, A.; Alkan, A.; Dogan, R.; Diaz-Aguilo, M.; De Leon, F.; Czarkowski, D.; Zabar, Z.; Birenbaum, L.; Noel, A.; Uosef, R.E. Experimental Determination of the ZIP Coefficients for Modern Residential, Commercial, and Industrial Loads. *IEEE Trans. Power Deliv.* **2014**, *29*, 1372–1381. [CrossRef]
52. Aziz, T.; Ketjoy, N. PV Penetration Limits in Low Voltage Networks and Voltage Variations. *IEEE Access* **2017**, *5*, 16784–16792. [CrossRef]
53. Barret, J.-P.; Bornard, P.; Mayer, B. *Power System Simulation*; Springer: Berlin/Heidelberg, Germany, 1996; Volume 288.
54. Snam; ARERA. *Descrizione Della Rete e Della Sua Gestione*; SNAM: San Donato Milanese, Italy, 2023.